Biological and Medical Applications of Materials and Interfaces

Fabrication of microporous coatings on titanium implants with improved mechanical, antibacterial and cell-interactive properties

Monica Thukkaram, Renee Coryn, Mahtab Asadian, Parinaz Saadat Esbah Tabaei, Petra Rigole, Naveenkumar Rajendhran, Anton Nikiforov, Jacob Sukumaran, Tom Coenye, Pascal Van Der Voort, Gijs Du Laing, Rino Morent, Alexander Van Tongel, Lieven De Wilde, Patrick De Baets, Kim Verbeken, and Nathalie De Geyter

ACS Appl. Mater. Interfaces, **Just Accepted Manuscript** • DOI: 10.1021/acsami.0c07234 • Publication Date (Web): 12 Jun 2020

Fabrication of microporous coatings on titanium implants with improved mechanical, antibacterial and cell-interactive properties

Monica Thukkaram [1], Renee Coryn[1], Mahtab Asadian[1], Parinaz Saadat Esbah Tabaei[1], Petra Rigole[2], Naveenkumar Rajendhran[3], Anton Nikiforov[1], Jacob Sukumaran[3], Tom Coenye[2], Pascal Van Der Voort[4], Gijs Du Laing[5], Rino Morent[1], Alexander Van Tongel[6], Lieven De Wilde[6], Patrick De Baets[3], Kim Verbeken[7], Nathalie De Geyter[1]*

[1]Research Unit Plasma Technology (RUPT), Department of Applied Physics, Faculty of Engineering and Architecture, Ghent University, Belgium

[2]Laboratory of Pharmaceutical Microbiology, Faculty of Pharmaceutical Sciences, Ghent University, Belgium

[3]Soete Laboratory, Department of Electrical Energy, Metals, Mechanical Construction and Systems (EEMMeCS), Faculty of Engineering and Architecture, Ghent University, Belgium

[4]Centre for Ordered Materials, Organometallics and Catalysis (COMOC), Department of Chemistry, Faculty of Sciences, Ghent University, Belgium

[5]Department of Green Chemistry and Technology, Faculty of Bioscience Engineering, Ghent University, Belgium

[5]Orthopedic Surgery and Traumatology, Department of Human Structure and Repair, Faculty of Medicine and Health Sciences, Ghent University, Ghent, Belgium

[7]Department of Materials, Textiles and Chemical Engineering, Faculty of Engineering and Architecture, Ghent University, Belgium

ABSTRACT

The success of an orthopedic implant therapy depends on successful bone integration and the prevention of microbial infections. In this work, plasma electrolytic oxidation (PEO) was performed to deposit TiO_2 coatings enriched with Ca, P and Ag on titanium to improve its surface properties and antibacterial efficacy while maintaining normal biological functions and thus to enhance the performance of orthopedic implants. After PEO treatment, the surface of Ti was converted to anatase and rutile TiO_2, hydroxyapatite and calcium titanate phases. The presence of these crystalline phases was further increased with an increased Ag content in the coatings. The developed coatings also exhibited a more porous morphology with an improved surface wettability, roughness, microhardness and frictional coefficient. *In vitro* antibacterial assays indicated that the Ag doped coatings can significantly prevent the growth of both *Staphylococcus aureus* and *Escherichia coli* by releasing Ag^+ ions and the ability to prevent these bacteria was enhanced by increasing the Ag content in the coatings resulting in a maximal 6-log reduction of *E. coli* and a maximal 5-log reduction of *S. aureus* after 24 hours of incubation. Moreover, the *in vitro* cytocompatibility evaluation of the coatings exhibited that the osteoblast (MC3T3) cell integration on the PEO-based coatings were greatly improved compared to untreated Ti and no notable impact on their cytocompatibility was observed on increasing the amount of Ag in the coating. In conclusion, the coating with favorable physico-chemical and mechanical properties along with controlled silver ion release can offer an excellent antibacterial performance and osteocompatibility and can thus become a prospective coating strategy to face current challenges in orthopedics.

Keywords: Antibacterial, Ag-containing coatings, TiO_2, Hydroxyapatite, Osteoblast cells, Ti implants

1. INTRODUCTION

Titanium (Ti) and its alloys have been commonly used in osteosynthesis applications such as joint prostheses, bone fixation devices, bone plates and screws for many years owing to their excellent corrosion resistance[1]. However, Ti implants cannot adhere and integrate directly to bone due to their insufficient osseointegration and osteoconductive properties[2]. Furthermore, Ti implants are prone to bacterial adhesion and subsequent biofilm formation, leading to implant associated infections. Once the infection occurs, bacteria tend to accumulate in a self-produced polymeric matrix to form a biofilm on the implant surface, and cells in this biofilm are protected against the action of administered antibacterial agents. Consequently, such infections can lead to premature implant failure resulting in the need for revision surgery leading to high healthcare costs[3]. It has been reported that the annual rate of implant-associated infections in orthopedic implants is between 2% and 5% in recent years[4]. Thus, the two main areas of concern in implant therapy are implant associated infections and successful bone tissue integration. Hence, there is a compelling need to enhance the surface properties of Ti-based implants to prevent biofilm formation and to improve bone tissue integration.

To improve the antibacterial properties of Ti-based implants, several surface modification techniques have been developed ranging from incorporating antibiotics over incorporating organic antimicrobial agents such as chitosan, collagen, chlorhexidine to the incorporation of inorganic antibacterial nanoparticles such as silver, copper and gold and iron-oxide[5,6]. Among these antibacterial agents, silver nanoparticles (AgNPs) are widely known to exhibit antibacterial activity due to their strong and broad antibacterial spectrum[7]. The antibacterial activity of AgNPs is due to their ability to produce large amount of reactive oxygen species (ROS), free radical species which inhibit the respiration and growth of bacteria leading to bacterial death. Besides, the Ag^{+} ions released from AgNPs are also considered to be an important factor towards their antibacterial activity[8]. Although the exact mechanism of the antibacterial activity of AgNPs is still

not clear and under debate, it is believed that it is caused by synergistic effects of both AgNPs and released Ag^+ ions[9]. Because of their excellent antibacterial activity, AgNPs have been incorporated into various implant surfaces such as fracture fixation devices, heart valve prostheses, catheters as well as orthopedic and dental implants[10]. However, studies have also reported that AgNPs cause cytotoxicity on various mammalian cells in a dose-dependent manner[7]. In addition to this, AgNPs have a tendency to aggregate and due to this bacterial resistance towards silver was already observed[11]. For these reasons, in recent years, the Federal Drug Administration (FDA) and other agencies have expressed their concerns on antibacterial approaches incorporating AgNPs[12,13]. Therefore, it is important to harness the excellent antibacterial properties of Ag^+ without actually using AgNPs by for example delivering Ag^+ from silver acetate or silver nitrate present with a suitable matrix.

As stated earlier, another problem associated with Ti-based implants is their insufficient osteoconductivity . Osteoconductivity can, however, be improved if successful tissue integration occurs before bacterial adhesion takes place during the race for colonization of the implant surface. Thus, an ideal implant surface should be bi-functional as it should possess both antibacterial and osteoconductive properties. The osteoconductive performance of Ti-based implants can be improved by coating bioactive compounds on Ti to accelerate bone formation or by creating a micro-rough surface on the implant which enhances the implant anchorage by supporting bone ingrowth[14,15]. Hydroxyapatite (HA) with chemical formula ($Ca_{10}(PO_4)_6(OH)_2$) has been widely used for many years as an active bioactive implant coating due to its outstanding bioactivity. Furthermore, HA improves osseointegration, osteoblast proliferation, bone formation and reduces bone loss due to its chemical and structural resemblance to bone minerals[16]. Surface modification techniques that can successfully deposit HA coatings on Ti surfaces include plasma spraying, the sol-gel method, electrophoresis and sputtering[17,18]. Unfortunately, all these methods have difficulties to deposit a coating on complex-shaped surfaces. In addition, these methods also have

the disadvantage of poor bonding between the substrate and the coating which typically results in delamination of the HA coatings from Ti. These issues can be overcome by synthesizing a titanium dioxide (TiO_2) coating in a Ca- and P-containing electrolyte by means of plasma electrolytic oxidation (PEO) in which HA is formed simultaneously with TiO_2 during the coating process. PEO provides a plasma based electrochemical conversion of metal substrates into oxide ceramic layers in the presence of an electrolyte[19]. These ceramic coatings containing both elements of the metal substrate and elements of the electrolyte are typically produced when the applied voltage is above the dielectric breakdown voltage of the growing oxide film[20]. The ceramic oxide coatings produced on metal surfaces are microporous and rough which enables better performance of bone implants as they can improve the growth of bone tissue. In addition, the deposited oxide layers can provide a wide variety of mechanical, tribological, and antibacterial properties via the incorporation of several ions and particles present in the electrolyte[21].

Most of the past study on plasma electrolytic oxidation has focused, however, on investigating the influence of operational parameters on the surface properties of the coating[22]. In addition, most researchers have investigated either the antibacterial performance or the bioactivity of PEO coatings fabricated in silver-containing or HA particle-containing electrolytes, respectively[23–25]. To the best of the authors' knowledge, no study has ever been reported on the bi-functional character of PEO coatings by incorporating antibacterial Ag^+ ions together with osteconductive Ca and P ions on Ti implant surfaces. Therefore, the aim of this particular study is to synthesize porous bi-functional oxide coatings on Ti discs by means of PEO in a base electrolyte containing calcium acetate monohydrate, sodium dihydrogen phosphate dihydrate with and without the addition of different amounts of silver acetate as supplier of Ag^+ ions. A detailed physico-chemical analysis and mechanical properties of the deposited coatings are examined. In addition, the dose-dependent effect of silver on the *in vitro* antibacterial performance, protein interactions and osteoconductivity of the prepared coatings is also investigated.

2. MATERIALS AND METHODS

2.1 Titanium discs preparation

Commercially pure titanium discs (Grade 1, purity>99.8 wt%) with a diameter of 12 mm and a thickness of 3 mm purchased from L&D Techniek NV were used as substrates. Prior to the treatment, titanium discs were ground with grinding paper up to 1200 and polished after which they were ultrasonically cleaned with acetone, ethanol and distilled water.

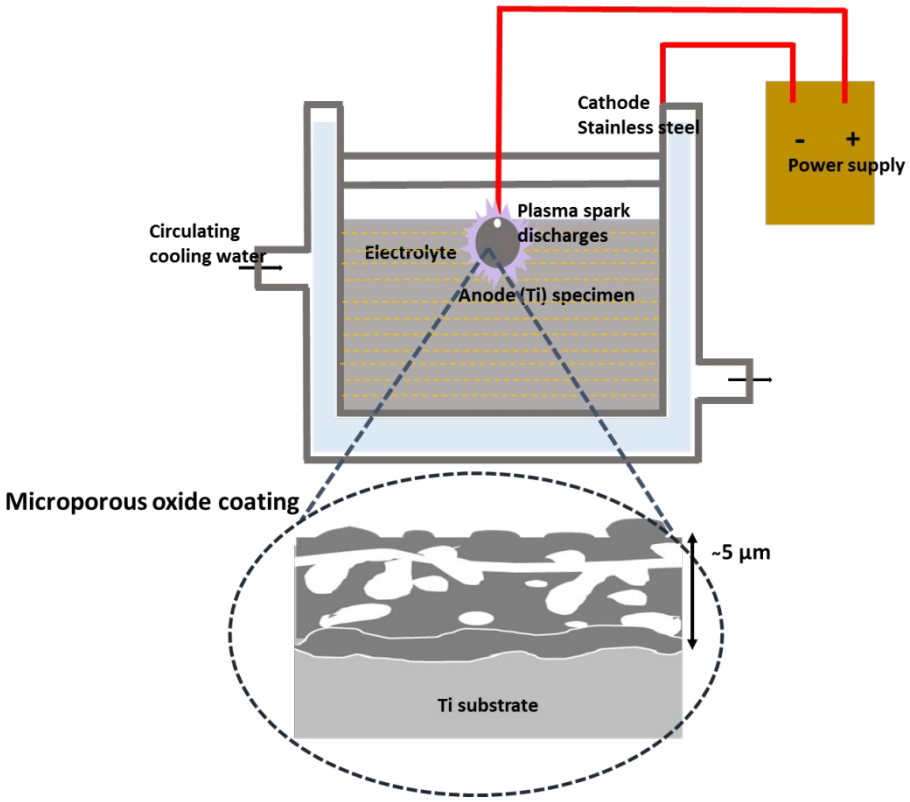

Figure 1. Schematic representation of the experimental device

2.2 PEO coatings deposition

A laboratory-scale in-house set up was customized for the PEO process as is schematically represented in **Figure 1**. The main components of the system are a DC power supply (DSC

electronics, DP15H-1D), a double-walled cylindrical stainless steel tank with two electrodes (stainless steel acts as a counter electrode and the Ti specimen as an anode) and a water cooling system (Julabo, F250) to maintain the temperature during the process. The electrolyte was prepared by dissolving 2.0 g of sodium dihydrogen phosphate dihydrate ($NaH_2PO_4.2H_20$) and 5.0 g of calcium acetate monohydrate ($Ca(OOCCH_3)_2$-H_2O) in 1L of distilled water with and without the addition of silver acetate ($AgOOCCH_3$) (concentrations of 0.1 g/L, 0.5 g/L and 0.8 g/L). These parameters were chosen to attain the ratio characteristic for stoichiometric HA (Ca/P = 1.6) which mimics the bone apatite properties[26]. 150 ml of the electrolyte was added to the double-walled stainless-steel electrolytic cell for the synthesis of the coatings. The temperature of the electrolyte was kept at 25 ± 5° C during the treatment to prevent chemical dissolution of the coating. The PEO synthesis was performed at a voltage of 500 V for 5 min. The variation in current density during the treatment with respect to the processing time is presented in **Figure S2** of the supplementary document showing that the current density after a treatment time of 5 minutes remained for all samples between 550 and 560 A/m^2**.** After the treatment, the coated Ti samples were washed with ethanol, distilled water and air-dried. Samples prepared in the Ag-free electrolyte and the Ag-doped electrolyte containing 0.1 g/L, 0.5 g/L and 0.8 g/L of $AgOOCCH_3$ will be referred to as the 0Ag, 0.1Ag, 0.5Ag and 0.8Ag samples, respectively.

2.3 Evaluation of the physico-chemical properties of the developed coatings

The surface and cross-sectional morphology of the PEO treated Ti discs were obtained using a JEOL JSM-6010 PLUS/LV SEM device (accelerating voltage - 7 kV, working distance - 11 mm) and a JEOL JSM-7600F field emission gun SEM device (accelerating voltage - 15 kV, working distance - 8 mm) respectively. In addition, cross-sectional elemental mapping of the coatings was also investigated with EDS present on the FEG-SEM device. Two independent samples were obtained for each condition using both microscopes.

XPS surface chemical analysis was performed using a PHI 5000 Versaprobe II spectrometer with a monochromatic Al K_α X-ray source (hν=1486.6 eV) operated at 25 W. Survey scans and individual high-resolution spectra of titanium (Ti2p), silver (Ag3d), oxygen (O1s), phosphorous (P2p) and calcium (Ca2p) were measured with a pass energy of 187.85 eV and 23.5 eV, respectively. For each sample, four spots were selected for measurements. The elements present on the coating were identified and quantified from the XPS survey scans using Multipak software (version 9.6.2). The high-resolution Ti2p, Ag3d, O1s, P2p and Ca2p peaks were also curve fitted using the Multipak software. The spectra were deconvoluted using Gaussian-Lorentzian peak shapes, keeping the FWHM (full width at half maximum) below 2 eV and the chi-square ($\chi 2$) value below 2.

A powder X-ray diffraction ARL X'TRA diffractometer (Thermo Scientific) with a Cu K_α (λ = 1.5405 Å) source was used to study the crystalline structure of the developed coatings. The device was operated using a 2θ value in the range of 20-80^o, an integration time of 1.2 s and a scan rate of 1° min^{-1}, respectively. The obtained XRD spectra were analyzed using the American mineralogist crystal structure database. XRD analysis was performed on 2 different samples per sample condition.

The surface wettability of the untreated and treated Ti discs was analyzed by WCA using a commercial contact angle goniometer (Krüss DSA25). Water droplets of 1 μL were placed on the Ti disc after which the WCA values were obtained by Laplace-Young curve fitting. For each condition, three different samples were analyzed (2 water drops/sample) and the mentioned WCA is the average of six obtained values.

2D roughness measurement of the Ti discs under study was performed using a Hommel somicronic surfacescan profilometer, using a tip radius of 2 μm and an opening angle of 90^o. The roughness parameter R_a was calculated according to DIN4776 standards. For each condition, four random locations were measured, and the mentioned R_a is the average of four obtained values

2.4 Evaluation of the coating mechanical properties

The surface hardness of the (un)coated Ti samples was measured using a Vickers hardness tester (Shimadzu HMV) with an applied load of 5 N on 10 random locations distributed over the entire sample surface and an average Vickers hardness number (VHN) per sample was calculated.

The frictional characteristics of untreated and PEO treated Ti discs were evaluated by performing single asperity microscale scratch test as shown in **Figure S1** of the supplementary information**.** Diamond indenter corresponding to Rockwell C scale with a tip radius of 200 μm and an included angle of 120° is used to experimentally simulate the scratches on the prepared specimen. A constant load ranging between 1 to 7 N was applied with a sliding velocity at 3 mm/s for 7 mm sliding distance at room temperature. Three replicate tests were performed for each sample and the average friction coefficient is reported in this work.

2.5 Silver ion release of the coatings

An inductively coupled plasma-mass spectrometer (ICP-MS, NexION 350) was used to analyze the Ag^+ release characteristics of the coatings. Prior to the analysis, the Ag-incorporated Ti discs were incubated into 20 mL of distilled water for different moments (3 h, 1 day, 3 days, 5 days and 7 days). After these moments, the released Ag^+ in the distilled water was analyzed using ICP-MS. Two independent tests were performed and the average Ag^+ value is reported in this work.

2.6 *In vitro* antibacterial assay

The antibacterial performance of the coatings under study was evaluated using *Escherichia coli* ATCC 25922, *Staphylococcus aureus* ATCC 6538 (methicillin susceptible, MSSA), and *S. aureus* Mu50 (methicillin resistant, MRSA). The colony forming units (CFU) was determined by the serial dilution method and the data were expressed as mean ± standard deviation based on 3 independent experiments (n=3). Additionally, the morphology of *S. aureus* Mu50 was also visualized using

SEM by fixing the bacterial cells after 24 h of incubation. A detailed description of the *in vitro* bacterial assay protocol can be found in section 1.2 of the supplementary information.

2.7 Protein adsorption assay by sodium dodecyl sulfate-polyacrylamide gel electrophoresis (SDS-PAGE)

In this study, bovine serum albumin (BSA) and fetal bovine serum (FBS) were used as model proteins to investigate *in vitro* protein interactions on (un)treated Ti discs by means of SDS-PAGE. In a first step, Ti discs were immersed in either a 10% FBS or a 2 mg/mL BSA solution in distilled H_2O for 2 hours at 37^oC. Afterwards, the samples were washed three times with distilled water and air dried to remove non-adherent proteins. Subsequently, all strongly adhered proteins were removed from the samples by incubating them in 1 mL of Laemmli buffer (62.5 x 10^{-3} M Tris – HCl, 2% SDS, 0.04 M β-mercapto-ethanol) supplemented with 0.01 % bromophenol blue at 100^oC for 4 min after which the supernatants were collected. Next, 10 µL of the supernatants was loaded onto a 10% SDS polyacrylamide gel (Bio-rad, Mini-Protean electrophoresis system, 100 V) to visualize the protein bands. The gels were collected once the bromophenol blue reached the end of the gel. Afterwards, a standard coomassie blue staining was performed followed by de-staining until the protein bands were clearly seen. The photographs of the gels were then taken, and the protein band intensities were measured using ImageJ software. Three replicate tests were performed for each sample and the average band intensities are reported relative to the control group of the corresponding protein (FBS, BSA). As an alternative, the samples under study were also immersed into a 0.5 mg/mL fluorescein isothiocynate (FITC)-labelled albumin solution in distilled H_2O for 1 h after which protein adsorption was visualized using an Olympus IX 81 fluorescence microscope with appropriate filters.

2.8 *In vitro* cell culture experiments

In addition to *in vitro* antibacterial and protein adsorption studies, the osteocompatibility of the coatings including cell adhesion and proliferation was also investigated as the cellular behavior of the coatings plays a important role in the final success of any implant material. Therefore, in this study, cell-material interactions on the fabricated coatings were examined 1 day and 7 days after seeding osteoblasts (MC3T3) using live/dead staining and MTT assays. Additionally, the morphology of fixed, dehydrated cells was also visualized using SEM. The detailed protocols used for the cell culture experiments are explained in detail in section 1.3 of the supplementary information.

2.9 Statistics

All *in vitro* experiments were performed on 3 independent samples (n=3) per sample condition and the data are represented as a mean with standard deviation. For statistical analysis, a one-way ANOVA combined with a Tukey post hoc test was utilized to determine the level of significance and a P value <0.05 was considered to be significant.

3. RESULTS AND DISCUSSIONS

3.1 Morphologies, chemical states and crystalline phases of the coatings

As a first step, the morphology of the coatings produced in this work was visualized by SEM. Figure **2A** and **B** shows the surface morphologies of silver free (0Ag) and silver incorporated TiO_2 coatings (0.1Ag, 0.5Ag, 0.8Ag) at different magnification. It can be seen that irrespective of the silver content all coatings were porous, a typical characteristic of coatings prepared by PEO. Similar results were also seen when using other electrolytes[5,27]. It can also be seen that the obtained pores were uniformly formed over the entire oxide layer and these porosities are due to the

electrical discharges that are formed on the surface of the samples. **Figure 3** shows the SEM-BSE cross-sectional (backscattered electrons) images of the Ag-free (0Ag) and Ag-incorporated coatings (0.1Ag, 0.5Ag and 0.8Ag). Based on these images, the deposited oxide layer's thicknesses were determined to be (5.0 ± 0.2) μm, (5.1 ± 0.3) μm, (5.2 ± 0.5) μm and (4.5 ± 1.8) μm for the 0Ag, 0.1Ag, 0.5Ag and 0.8Ag samples, respectively. Consequently, the final thickness of the deposited oxide layer was not affected by doping different amounts of silver acetate. From the EDS mapping (**Figure 4**), it can be seen that O, P and Ca were homogeneously distributed along the entire oxide coating surface. It can thus be observed that the deposited oxide coatings were enriched with both Ca and P, suggesting the possible presence of calcium titanates and/or titanium phosphates[24]. From the Ag mapping, it also becomes apparent that Ag did not form any aggregates in the oxide layer which is commonly observed when incorporating other forms of Ag in the electrolyte[5,24]. This finding is very positive as a uniform deposition of Ag in the oxide layer is essential to have a constant release of Ag^+ which can in turn provide a better antibacterial performance as aggregates of silver are known to lead to bacterial resistance[11].

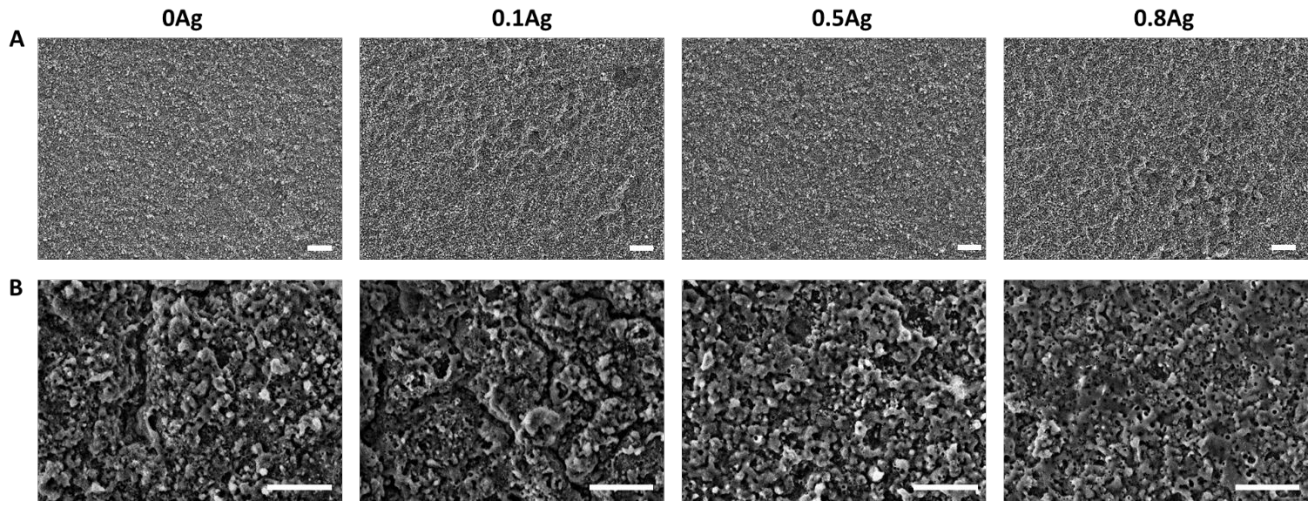

Figure 2. Surface SEM images of the coatings at scale bar: 10 μm (A) and scale bar: 5 μm (B).

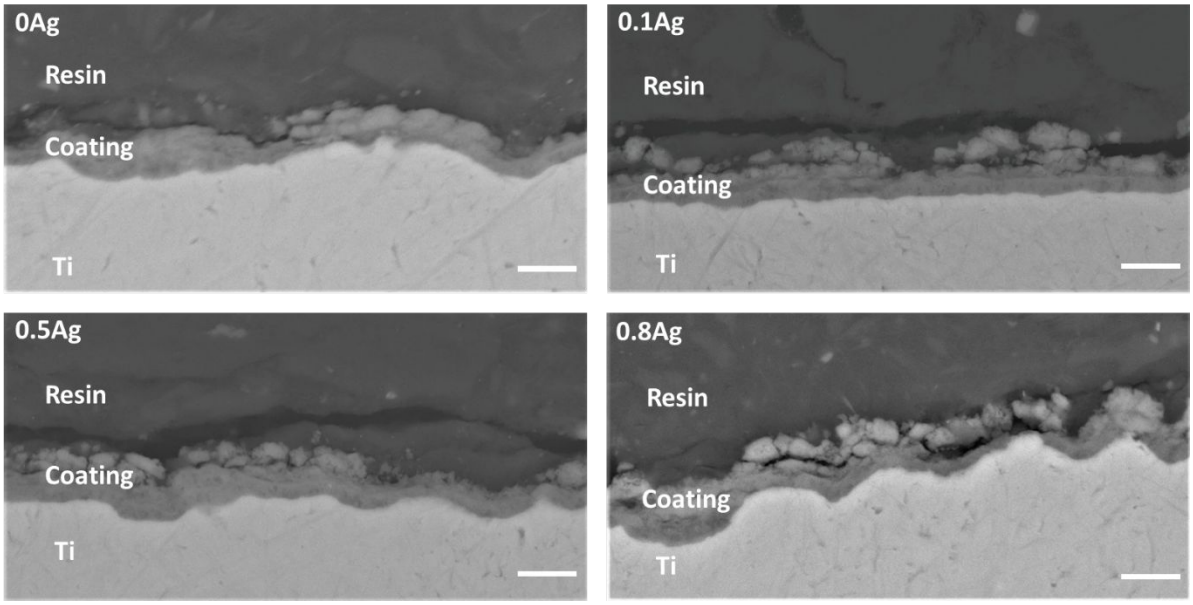

Figure 3. Cross-sectional SEM-BSE images of the coatings (Scale bar: 5 μm).

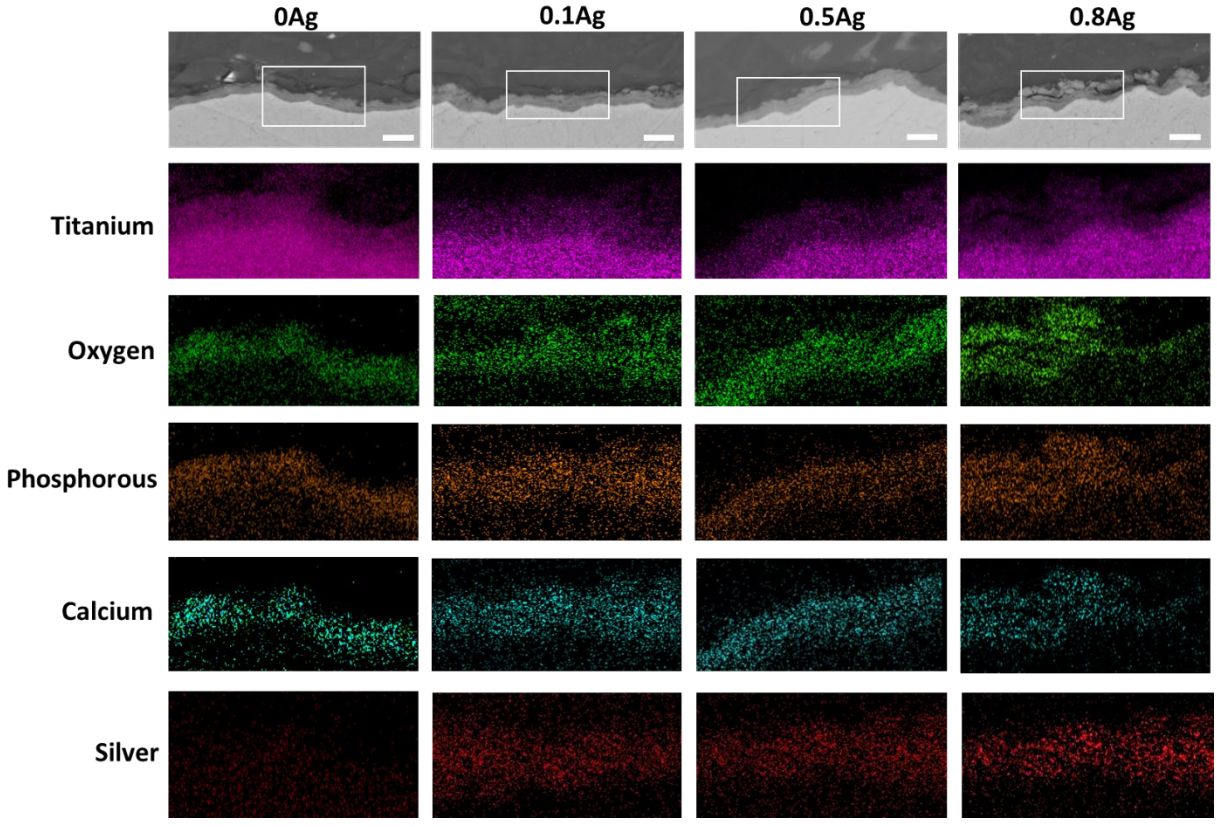

Figure 4. Cross-sectional SEM-BSE images and EDS elemental mapping corresponding to the marked area in the upper SEM-BSE images of the coatings (Scale bar: 5 μm).

To explore the surface chemical composition of the coatings, the coatings were examined by XPS. **Figure 5** shows the XPS survey spectra of 0Ag, 0.1Ag, 0.5Ag and 0.8Ag coatings. The surface of all studied coatings consisted out of Ti, O, Ca, P and C, which is in agreement with the previously shown EDS mapping results. For the Ag-doped coatings (0.1Ag, 0.5Ag, 0.8Ag), a peak attributed to the element Ag was also detected in the XPS survey spectra and the intensity of these Ag peaks increased with increasing silver acetate content in the electrolyte. The surface elemental composition of the coatings was determined from these survey spectra and the obtained results are shown in **Table 1**. The data clearly show that the surface elemental composition of all studied coatings was similar, with the exception of the silver content. As expected, silver was not observed at the surface of the 0Ag sample, in contrast to the samples 0.1Ag, 0.5Ag and 0.8Ag. A small (though not significantly different) increase in Ag content with increasing silver acetate content in the electrolyte was also observable. This relatively small Ag concentration was the result of the limited penetration depth of XPS as in the case of AlK_{α} radiation, the sampling depth of XPS is typically in the range 3-10 nm while the thickness of the coating is in the order of µm's. Consequently, only the Ag that was present in the close proximity of the surface of the oxide films contributed to the XPS signal and Ag that was buried deeper inside the porous layer was thus not detected. **Figure 5(B-F)** shows the high-resolution XPS spectra of the elements titanium (Ti2p), silver (Ag3d), oxygen (O1s), phosphorous (P2p) and calcium (Ca2p) of the coating surface of the sample 0.8Ag. As there was no significant difference in the obtained high-resolution spectra among all Ag-doped samples under study, only the high-resolution XPS peaks of the sample 0.8Ag are presented in this work. As it can be seen in **Figure 5B,** the Ti2p spectrum contained two well-separated peaks at 464.5 eV for $Ti2p_{1/2}$ and 458.8 eV for $Ti2p_{3/2}$, a doublet which is known to correspond to titanium dioxide[28]. The Ag3d high-resolution spectrum **(Figure 5C**) also consisted out of 2 well-defined peaks centered at 368.2 eV for $Ag3d_{5/2}$ and 374.2 eV for $Ag3d_{3/2}$ with a binding energy difference of 6 eV between both peaks indicating the presence of metallic silver[29].

The broad O1s spectrum (**Figure 5D**) could be deconvoluted into three Gaussian components[30]. The peak located at 530.1 eV was assigned to oxygen in TiO_2[31] and O atoms bound to other atoms such as Ca and Ag. The second peak at 531 eV corresponded to oxygen present in titanium phosphates while the third peak at 532.2 eV was associated to oxygen present in the chemical groups Ti-OH and P-OH. The broad P2p spectrum (**Figure 5E**) of the 0.8Ag coating could be deconvoluted into 2 separate peaks: one at 132.8 eV and one at 133.5 eV which could be attributed to P-O bonds in PO_4^{3-} and HPO_4^{2-}, respectively[32]. Finally, the high-resolution Ca2p spectrum (**Figure 5F**) was deconvoluted into two separated peaks located at 347.1 eV and 350.7 eV, which could be attributed to calcium present in $Ca_3(PO_4)_2$[33]. From the deconvoluted spectra, it can thus be observed that the developed coating surface was consisted of TiO_2 containing a small amount of calcium and phosphate groups. The Ca and P elements in the coatings mainly existed as $Ca_3(PO_4)_2$, regardless of the amount of Ag incorporation. However, as already stated, the XPS results can only provide chemical information of the top few nm's of the coating, therefore, XRD analysis was also performed to additionally investigate the crystallinity of the developed coatings.

Table 1. Elemental composition of the coatings obtained from XPS analysis

Sample	Ti (at%)	O (at%)	Ca (at%)	P (at%)	C (at%)	Ag (at%)
0Ag	5.7 ± 1.1	54.6 ± 2.3	9.7 ± 1.6	6.2 ± 2.1	23.9 ± 3.5	0
0.1Ag	4.7 ± 1.3	55.2 ± 1.6	10.3 ± 0.6	7.1 ± 1.1	21.9 ± 1.6	0.8 ± 0.5
0.5Ag	4.2 ± 1.2	54.2 ± 1.8	10.7 ± 1.5	6.5 ± 0.8	22.9 ± 1.9	1.5 ± 0.8
0.8Ag	4.3 ± 1.6	53.1 ± 1.8	9.6 ± 1.1	6.6 ± 0.9	24.3 ± 1.7	2.2 ± 1.5

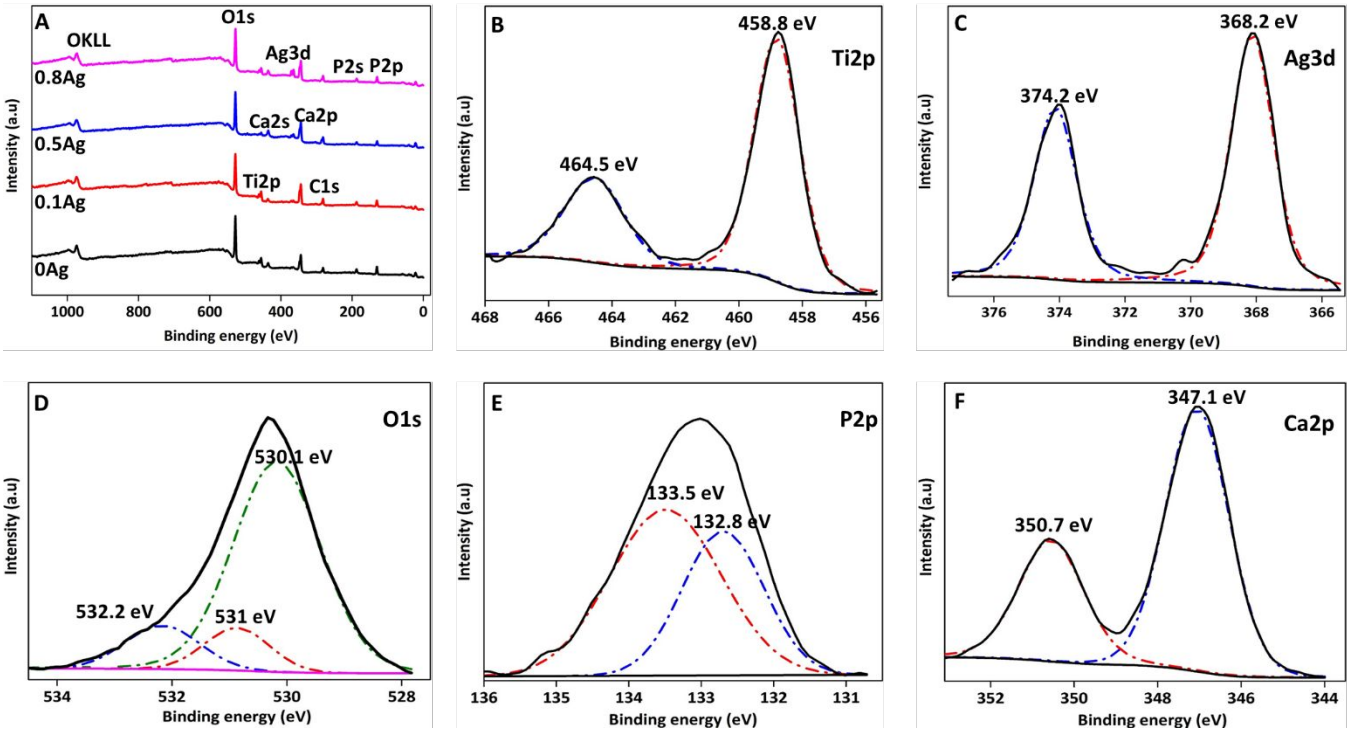

Figure 5. XPS survey spectra of the coatings (A), deconvoluted high-resolution Ti2p (B), Ag3d (C), O1s (D), P2p (E) and Ca2p (F) peaks of the 0.8Ag coating.

XRD patterns of PEO-treated Ti discs were obtained and the gathered results are shown in **Figure 6.** The coatings primarly composed of the rutile and anatase forms of titanium dioxide (TiO_2), hydroxyapatite and calcium titanate ($CaTiO_3$). The peaks intensities changed depending on the silver acetate concentration of the electrolyte used during the PEO process. As can be seen in **Figure 6**, with an increased silver concentration in the electrolyte, the peak intensities of the rutile phase (2θ = 28.1, 35.06, 36.2) were increased in comparison to anatase phases (2θ = 25.2) along with an increase in peak intensities of the hydroxyapatite (2θ = 27.46, 31.66, 39.7, 44.6) and $CaTiO_3$ (2θ = 47.04, 49.48) phases. This effect was more noticeable for the 0.5Ag and 0.8Ag samples. Therefore, it can be stated that the 0.5Ag and 0.8Ag samples contained more rutile TiO_2 and Ca- and P-containing phases (hydroxyapatite and $CaTiO_3$) compared to the 0Ag and 0.1Ag samples. Similar to our findings, Muhaffel et al.[24] also reported more intense hydroxyapatite and rutile phase formation in the coatings when using an increased concentration of $AgNO_3$ in the electrolyte. Similarly, Song et al. [34] reported the formation of Ca- and P-containing phases such as hydroxyapatite and tricalcium phosphate and observed that the appearance of the hydroxyapatite phases was dependent on the $AgNO_3$ or CH_3COOAg concentration used in the electrolyte. The observed differences in crystallinity are due to the fact that increasing the silver content in the electrolyte leads to a PEO process proceeding at higher current density thereby enhancing the crystallinity of the deposited TiO_2 layer (see **Figure S2** of the supplementary information).

Thus, during PEO, different crystalline phases can be obtained by varying the composition of the electrolyte. At the first step of the PEO process, Ti and hydroxyl ions react with one another to form anatase and rutile phases in the microdischarge channels. The anatase phase is formed earlier when the temperature is low in the microdischarge channels hence it is thermodynamically less stable than rutile. Both anatase and rutile phases can form bioactive hydroxyl apatite layers and have good biocompatibility towards different cell types[35]. At the next step of the PEO process,

calcium and phosphate ions occurring at a higher temperature in the microdischarge channels react with each other to form hydroxyapatite phases in the coating while calcium titanate phases are formed by the reaction of calcium, titanium and hydroxyl ions[36]. Studies have demonstrated that calcium titanate layers can contribute to an increased adhesion strength between Ti and hydroxyapatite and can decrease the progression of hydroxyapatite dissolution in an acidic environment which is produced by osteoclastic resorption in the body[36,37]. It is therefore presumed that the presence of these crystalline phases on the coating surface may positively influence the bioactivity and biocompatibility of Ti by improving its osteogenic properties.

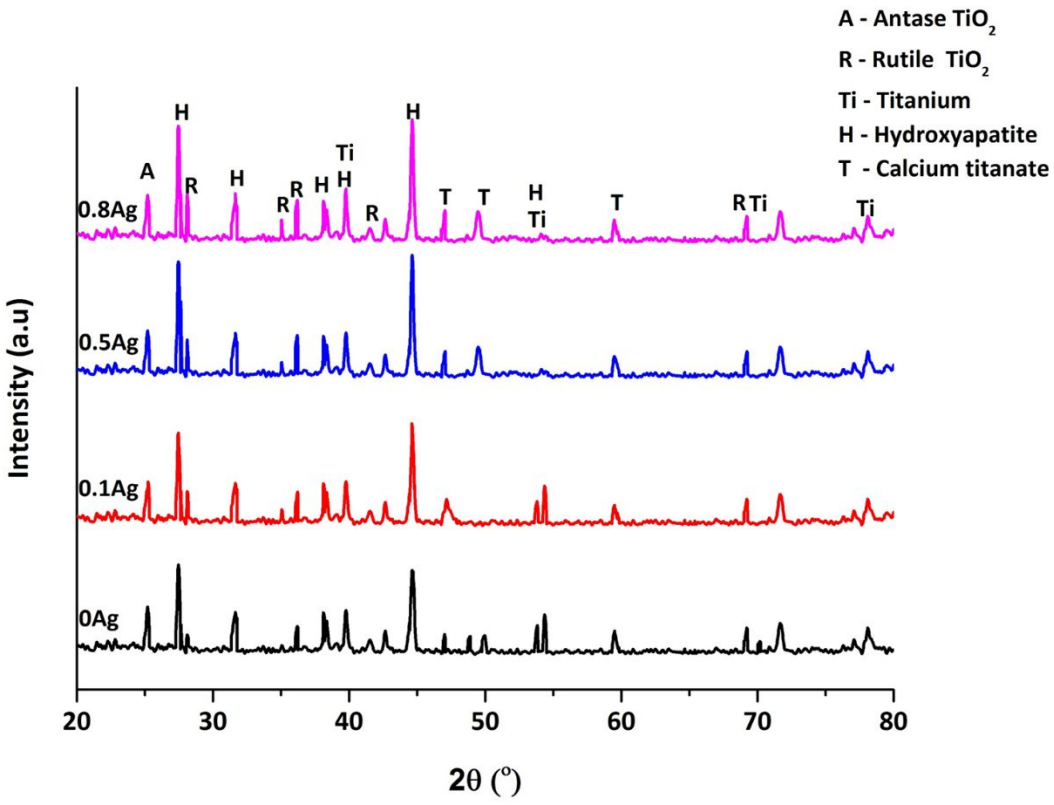

Figure 6. XRD spectra of 0Ag, 0.1Ag, 0.5Ag and 0.8Ag coatings.

3.2 Surface roughness, wettability and microhardness

The average roughness values (R_a) of the pristine polished titanium surface and the 0Ag, 0.1Ag, 0.5Ag and 0.8Ag coatings are shown in **Figure 7A.** The originally very low surface roughness of

the polished Ti disc strongly increased after all conducted PEO processes. The observed increase in surface roughness could be attributed to the formation of porous coatings on top of the smooth Ti substrate during the PEO process. Meanwhile, after the PEO processes, the WCA of the samples significantly decreased from 60^{o} for the untreated Ti disc to approximately 22^{o} for all coated samples (**Figure 7B**). The R_a and WCA of the silver-doped coatings (0.1Ag, 0.5Ag and 0.8Ag) were comparable to those of the silver-free coating (0Ag), indicating that the Ag incorporation in the coatings did not change their surface microstructure nor wettability. Similar findings were observed by Zhang et al.[38]. The microhardness of the untreated Ti and PEO-treated Ti samples is shown in **Figure 7C.** While the microhardness of the untreated Ti was approximately 200 VHN, the microhardness of the PEO-treated samples was much higher (400-500 VHN). The difference in microhardness between the untreated and coated Ti substrates could be attributed to the porous morphology (hard ceramic oxide layers) and the crystallinity (rutile phases) of the deposited coatings[39]. Although there was no significant difference in microhardness between the different PEO coatings, a slight increase in microhardness was observed for the samples 0.5Ag and 0.8Ag in comparison to the samples 0Ag and 0.1Ag. This increase may be due to the higher amount of rutile phases (as observable in **Figure 6**) in the former samples. The observed increase in sample surface hardness is very beneficial for clinical applications, as it decreases the occurrence of wear of an implant and thus contributes to its longevity[40].

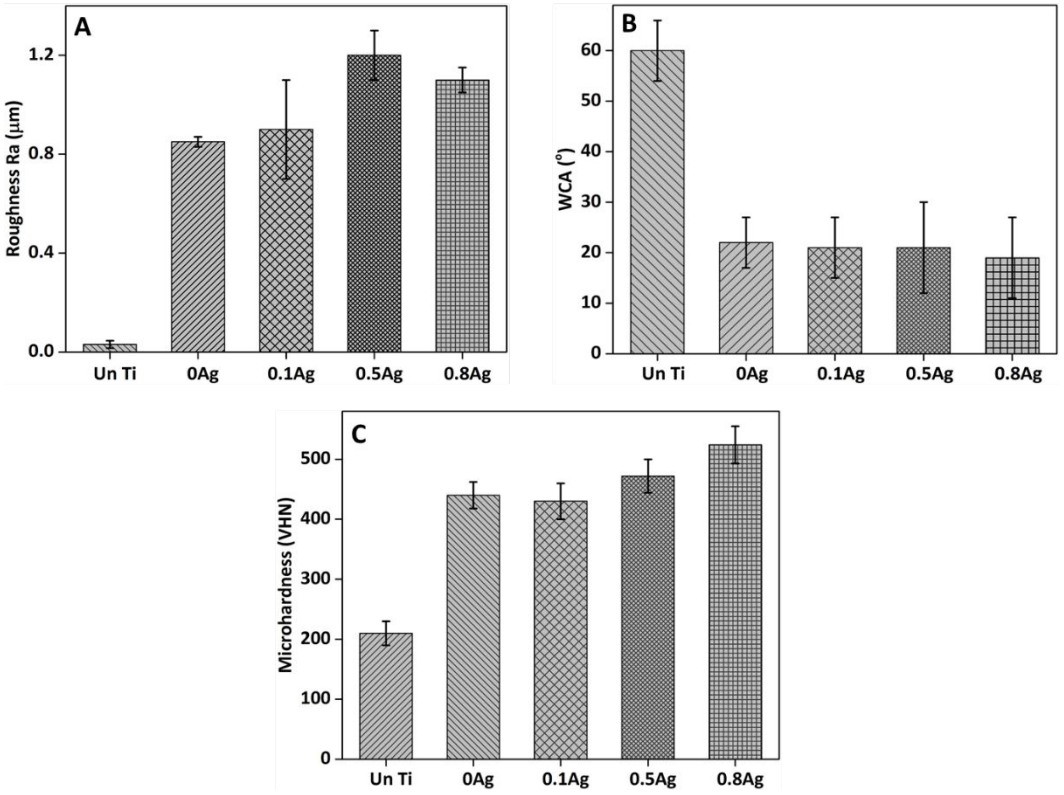

Figure 7. Roughness (A), WCA (B) and microhardness (C) of uncoated and coated Ti samples

3.3 Frictional coefficient of the coatings

To evaluate the frictional coefficient of the untreated and PEO-treated Ti discs, the scratch test using a diamond indenter at various loads is used and the results are illustrated in **Figure 8**. As shown, all PEO-treated coatings exhibited a lower frictional coefficient compared to the untreated Ti at all examined loads. This decrease could be explained by the increased hardness of the deposited ceramic-like coatings (see **Figure 7C**). However, the frictional coefficient was also reduced when the Ag concentration in the electrolyte was increased (0.5Ag, 0.8Ag) and the decrease was more pronounced at higher loads (5 N and 7 N). A similar trend was also observed for coatings containing alumina and silica particles prepared by PEO[41] and for silver tantalate coatings[42]. This frictional coefficient decrease may be either due to the increased crystallinity[43] of the 0.5Ag and 0.8Ag coatings or due to lowest contact resistance offered by Ag containing surface[44]. Besides, the silver content in the coating may act as a lubricant between the indenter and

Ti substrate, thus reducing the frictional coefficient [41,42,45]. Although coatings with high frictional coefficient are considered to be an advantage in providing primary fixation for implants, the prominent factors causing implant loosening are considered to be particle accumulation and failure in osseointegration[46]. Moreover, coatings with a high frictional coefficient can also generate wear debris, leading to inflammation which is in turn destructive to the bone supporting the implant. The observed decrease in the frictional coefficients of the PEO-treated samples might thus be favorable for implant applications, as the coatings might increase the resistance to wear and consequently decrease the occurrence of implant loosening[47,48].

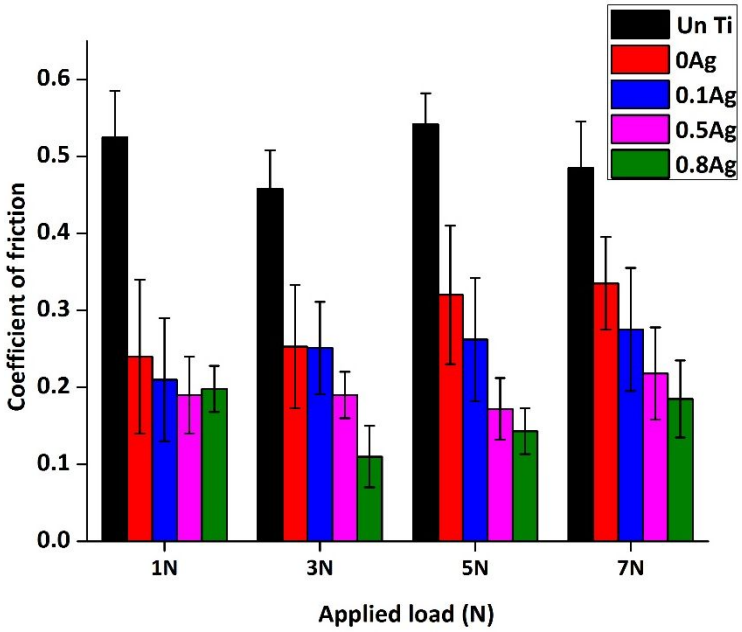

Figure 8. Coefficient of friction of untreated and PEO-treated Ti discs evaluated by a scratch tester at varying loads.

3.4 Ag^+ ions release kinetics

The Ag^+ release kinetics of the silver doped samples (0.1Ag, 0.5Ag, 0.8Ag) were investigated using ICP-MS by incubating the samples in water for up to 7 days. The result of this test is summarized in **Figures 9A and B** where the Ag^+ cumulative release profiles and the Ag^+ release

per day of 0.1Ag, 0.5Ag and 0.8Ag samples are plotted as a function of incubation time in water. As can be seen in F**igure 9A**, the cumulative Ag^+ release was observed to increase with incubation time for all Ag-doped samples. However, the increase was much less pronounced for the 0.1Ag sample compared to the coatings containing higher amounts of silver (0.5Ag and 0.8Ag). Samples with a higher Ag concentration present in the coating (0.5Ag, 0.8Ag) exhibited a higher Ag^+ release at any given point throughout the total incubation time of 7 days. The maximum amount of Ag^+ released from the 0.1Ag, 0.5Ag and 0.8Ag samples in cumulative measurements over 7 days was approximately 264 ppb, 813 ppb and 1110 ppb, respectively. As expected, the actual amount of released Ag^+ was thus strongly affected by the initial silver loading, and also strongly depended on the incubation time. This observation was in agreement with previously reported release results for other oxide coatings[23,24]. As shown in **Figure 9B**, the release of Ag^+ per day (ppb/day) after the first immersion day was 30 ppb/day, 84 ppb/day and 112 ppb/day for the 0.1Ag, 0.5Ag and 0.8Ag coatings, respectively. The Ag^+ release per day of the 0.1Ag sample was observed to increase during the first day of immersion after which a constant level of release was observed followed by a decrease in the Ag^+ release after 7 days of immersion. On the other hand, for the 0.5Ag and 0.8Ag samples, the Ag^+ release was found to decrease after 3 days of immersion. Thus, these samples showed an initially increasing Ag^+ release reaching a peak release after 3 days immersion, followed by a lower Ag^+ release. Additionally, it can also be observed that the Ag^+ release for the 0.1Ag and 0.8Ag samples was lower at day 7 than at day 5, whereas a slight increase in Ag^+ release was observed for the 0.5Ag sample on day 7 compared to day 5. This opposite trend may be due to the slightly different arrangement of silver within the oxide layer in case of sample 0.5Ag as the release kinetics of the prepared coatings are known to mainly depend on the diffusion pathway of silver present in the porous coatings. Silver present closer to the surface releases Ag^+ more quickly due to its shorter diffusion path (initial Ag^+ release) while silver present deeper in the porous oxide coating is released at later time points as this release is diffusion limited.

Consequently, the slight increase in Ag^+ release for the sample 0.5Ag on day 7 might be due to the particular arrangement of silver within this porous oxide layer, which is unfortunately an uncontrollable factor in the case of PEO.

Concerning the optimal amount of Ag^+ desired to achieve excellent biocompatibility and antibacterial ability, Shi et al. reported that an Ag^+ concentration between 270 ppb and 2200 ppb exhibited 90% antibacterial efficiency against *E. coli* and *S. aureus* and 80% cell viability of fibroblast cells. However, increasing the Ag^+ concentration above 2200 ppb showed an increase in bacterial reduction combined with a decrease in cell viability[49]. Similarly, no cytotoxic reaction of human mesenchymal stem cells was observed with a Ag^+ concentration below or equal to 1000 ppb[50]. On the other hand, the minimum inhibitory Ag^+ concentrations for *E. coli* and *S. aureus* are 0.3 ppb and 3.5 ppb. In this respect, Ag^+ rates from the coated samples prepared in this work are sufficient for killing bacteria without negatively affecting cells. However, additional studies have to be performed to evaluate the long-term release characteristics of Ag^+ from the prepared coatings.

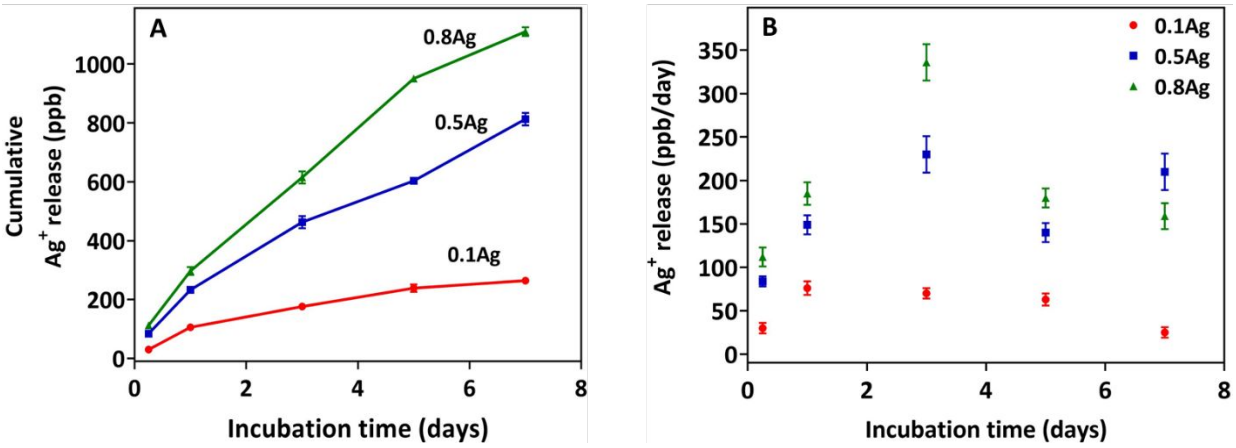

Fig. 9. Cumulative Ag^+ release (ppb) (a) and Ag^+ release rate (ppb/day) when incubated in water up to 7 days for 0.1Ag, 0.5Ag and 0.8Ag samples.

3.5 Antibacterial efficiency of the coatings

The antibacterial assays against *E. coli* (ATCC 25922*)*, MSSA ATCC 6538) and MRSA (Mu50) were performed on the studied samples and the untreated Ti disc served as control. These bacterial species were selected as representatives of Gram-negative and Gram-positive bacteria and because they are commonly found in implant associated infections. As can be seen in **Figure 10**, no reduction in *E. coli*, MSSA and MRSA was observed when untreated Ti and Ag- free coatings (0Ag) were tested. In both cases, approximately 10^8 CFU were recovered for all three bacterial strains after 24 hours of incubation. In contrast, the Ag-doped (0.1Ag, 0.5Ag, 0.8Ag) coatings showed a significant reduction ($P < 0.05$) in bacterial cell numbers. The antibacterial efficiency of the coatings was strongly dependent on the concentration of silver acetate in the electrolyte during the PEO treatment process. In the case of samples with low Ag content (0.1Ag), a 4-log reduction of *E. coli*, a 3-log reduction of MSSA and a 2-log reduction of MRSA were observed. Samples with high Ag content (0.5Ag, 0.8Ag) exhibited an even superior antibacterial activity showing approx. a 6-log reduction of *E. coli* and a 5-log reduction of MSSA and MRSA after 24 hours of incubation. These findings, i.e. the decrease in bacterial numbers with increasing concentration of silver acetate in the electrolyte corresponded well with the measured Ag^+ release (**Figure 9**) and suggested that the Ag^+ released from the coatings into the neighboring aqueous medium were the main antibacterial compounds[51]. In fact, studies have reported that the mechanism of antibacterial action of Ag^+ is jointly associated with its interface with thiol groups in enzymes and proteins[52]. Sondi et al. observed cells of *S. aureus* and *E. coli* exposed to Ag^+ by means of transmission electron microscopy and observed that after exposure the cellular content of the bacteria was released from the cell wall and consequently the cell wall was degraded[53]. Although the exact mechanisms underlying the antibacterial mechanism of Ag^+ are still not fully understood, many previous studies reported that the interaction between Ag^+ and bacterial membranes can cause structural damage to the membranes and the cell metabolic activity resulting into cell death[52,54].

In addition to the antibacterial assays, SEM examination of MRSA was also performed to investigate the effect of Ag incorporation in the coatings on the bacterial adhesion and morphology of MSRA colonies. From **Figure 11,** it can be seen that the adherent *S. aureus* started to form a biofilm as they clustered on the untreated Ti surface and the 0Ag coating, but these bacterial clusters were decreased with increased dose of Ag^{+}. MRSA cells displayed a round-shaped morphology and undamaged binary fission (indicated by the blue arrows in the inset SEM images of samples Ti, 0Ag and 0.1Ag) when cultured on the untreated Ti surface (Ti), the Ag-free coating (0Ag) and the coating with the lowest Ag content (0.1Ag). While the cells look intact and display smooth surfaces on the untreated Ti surface and the 0Ag sample, distinct cell debris and lysed cells (red arrows in the inset SEM images of samples 0.1Ag, 0.5Ag and 0.8Ag) were also observed on the silver-incorporated 0.1Ag, 0.5Ag and 0.8Ag coatings. In addition, no undamaged binary fission was observed on the 0.5Ag and 0.8Ag samples. Combined, these results indicated that the Ag-doped coatings exhibited a greater ability to inhibit both Gram-positive and Gram-negative bacteria and the coatings with increased Ag content had superior antibacterial efficacy against all investigated bacteria.

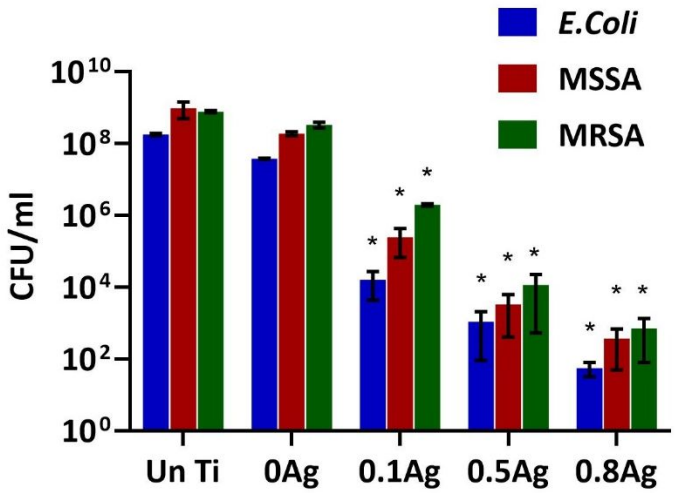

Figure 10. Number of CFU after 24 hours of incubation for different samples. Asterisk (*) denotes a significance difference at $P < 0.05$ compared to the control sample (untreated Ti).

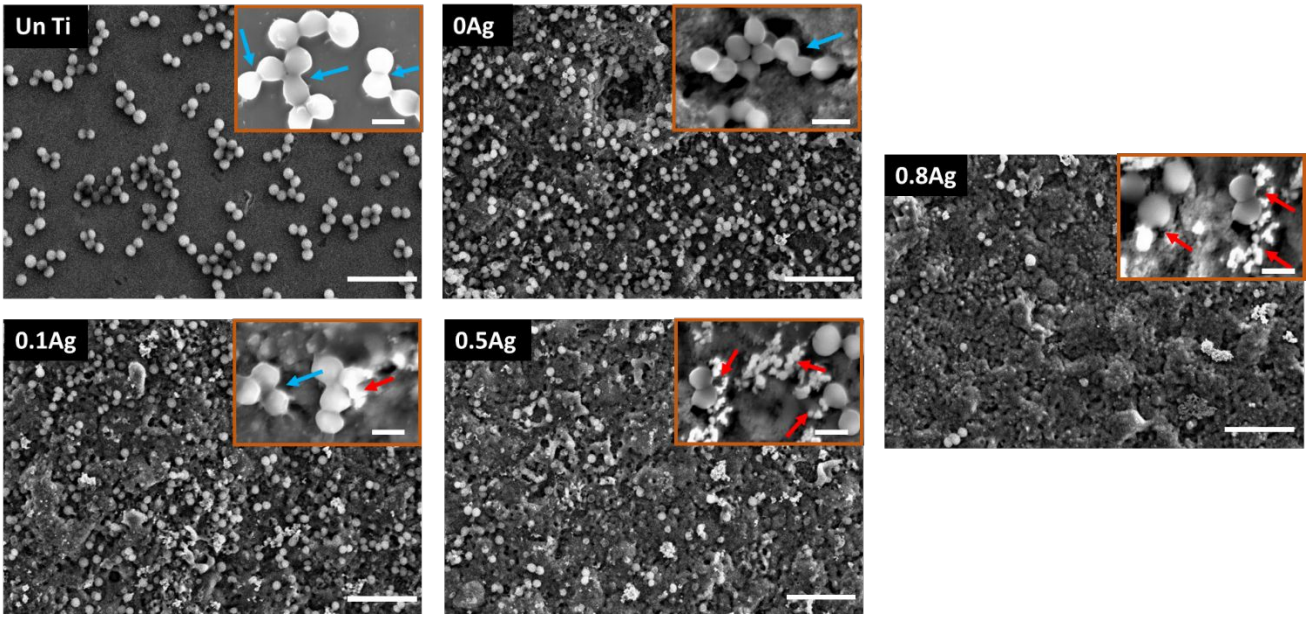

Figure 11. SEM images of MRSA strain cultured on uncoated and coated Ti samples (scale bar: 5 µm, insert : 1 µm).

3.6 Protein adsorption to the coatings

When a foreign material is placed in the body, the first mechanism that takes place within the first few hours of implantation is the deposition of a protein layer from the blood and the body fluids onto the implant surface[55]. The presence of this film influences the interactions between the material and the cell/bacteria together with the activation of inflammatory reactions[56]. Therefore, it is important to investigate the protein adsorption on the implant material and for this purpose, FBS and BSA were used as model proteins. **Figures 12A and B** show the images of the obtained SDS-PAGE gels and the percentage of the band intensities (relative to the control samples FBS and BSA, respectively). As can be seen, in case of FBS, no protein band was present for the untreated Ti whereas a very light band was observed for the samples 0Ag, 0.1Ag and 0.5Ag and a strong band for the 0.8Ag sample. This finding thus suggests that FBS adsorption was the most pronounced on the 0.8Ag sample. A similar trend was seen for samples exposed to BSA, while in

this particular case the intensity of the BSA band strongly increased on the samples 0.5Ag and 0.8Ag. Thus, a preferential adsorption of albumin (molecular weight – 64 kDa) was observed on all PEO-treated samples with the most pronounced adsorption on the 0.5Ag and 0.8Ag samples at the early phase of the formation of a protein layer (after 2h immersion). A similar effect was seen on the fluorescence images of samples incubated in FITC-labelled albumin (see **Figure S3** of the supplementary information). These results are in agreement with Chen at al., who reported that an Ag^{+} release up to 1.7 ppm did not have any deleterious effect on protein structure or protein adsorption[57].

Albumin adsorption on the surface was observed to be beneficial for biomaterials, as pre-adsorption of albumin inhibits platelet adhesion and hence inhibits inflammatory reactions[56,58]. Between the PEO-treated and the untreated Ti, an increased albumin adsorption observed in the former was mainly related to the surface physico-chemical properties such as changed chemical composition as well as improved wettability, roughness and crystallinity which was in agreement with previously published results[56]. However, among the PEO-treated coatings (0Ag, 0.1Ag, 0.5Ag and 0.8Ag), the observed difference in albumin adsorption was mainly due to the increased amount of Ag on the coating surface and the increased crystallinity as all coatings exhibited a similar wettability (WCA – 20^{o}) and surface roughness (~1 μm). Thus, the observed increase in albumin adsorption on the coatings containing high amounts of silver was due to the fact that these coatings possess more binding sites as disulfide bonds present in the albumin can form strong sulfur-silver complexes[59]. Moreover, the presence of $Ca^{2+}$and PO_4^{3-} ions in the coatings under study are also believed to be albumin binding sites and thus provide a major driving force for its adsorption[60,61].

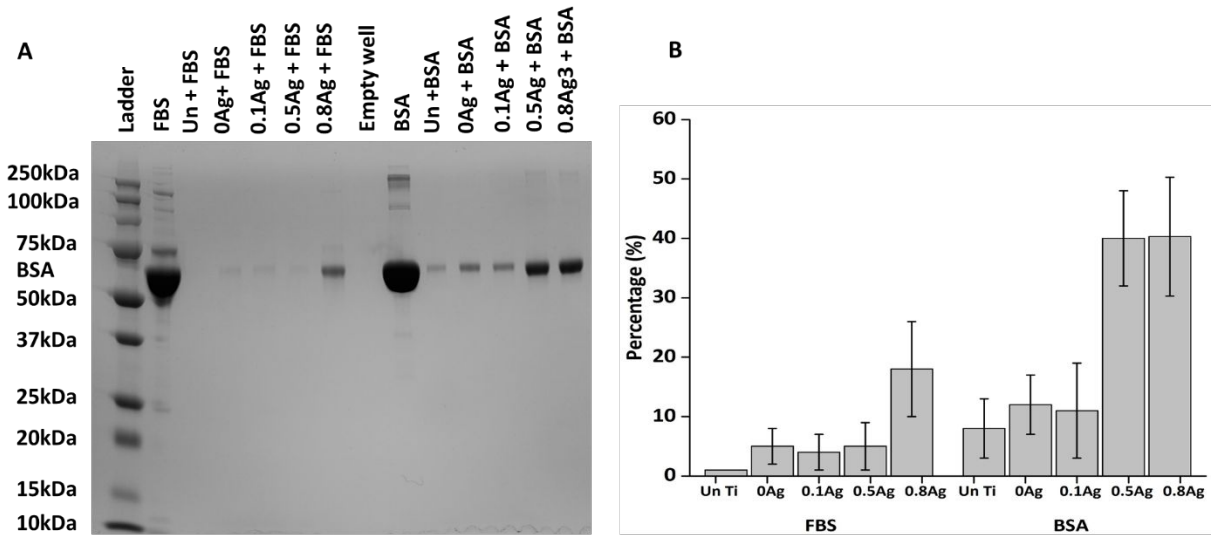

Figure 12. SDS-PAGE analysis of FBS and BSA proteins for different Ti samples under study: (A) gel image of one of the triplicate measurements showing the protein bands (A) and percentage of the intensity of the FBS/BSA bands calculated from the gel images using ImageJ (B).

3.7 Osteoblast cell response

Besides examining the surface characteristics, the *in vitro* antibacterial properties and protein adsorption of the produced coatings, the cellular behavior was also investigated to understand the relationship between the coating's surface properties, the Ag content of the coatings and their cellular response. In the first step, the morphology and viability of MC3T3 cells cultured on both untreated and PEO-treated Ti samples were examined by SEM and fluorescence microscopy after live/dead staining of the cells. **Figure 13 and Figure 14** show the SEM and live/dead images that were obtained on day 1 and day 7 after cell seeding, respectively. These images clearly exhibited differences between the untreated Ti sample, the Ag-free (0Ag) and the Ag-incorporated (0.1Ag, 0.5Ag, 0.8Ag) coatings. As it is shown in **Figure 13** (1st and 2nd column), one day after cell seeding,

the MC3T3 cells adhering to the untreated Ti sample exhibited a rather round morphology implying limited cell adhesion. In contrast, the amount of adhered cells was significantly higher on all PEO-treated samples compared to the untreated Ti. Moreover, on these samples, the MC3T3 cells were more elongated and spindle shaped suggesting excellent cell adhesion. From the fluorescence images (3rd column), it can be observed that one day after cell seeding, nearly no dead cells were noticed on the surface of all samples implying that the coatings deposited on the Ti substrate had no detectable cytotoxicity to osteoblast cells. In fact, the Ag-free and Ag-doped coatings exhibited a higher cell density with more living cells independently of the Ag content in the coating as compared to the untreated Ti surface.

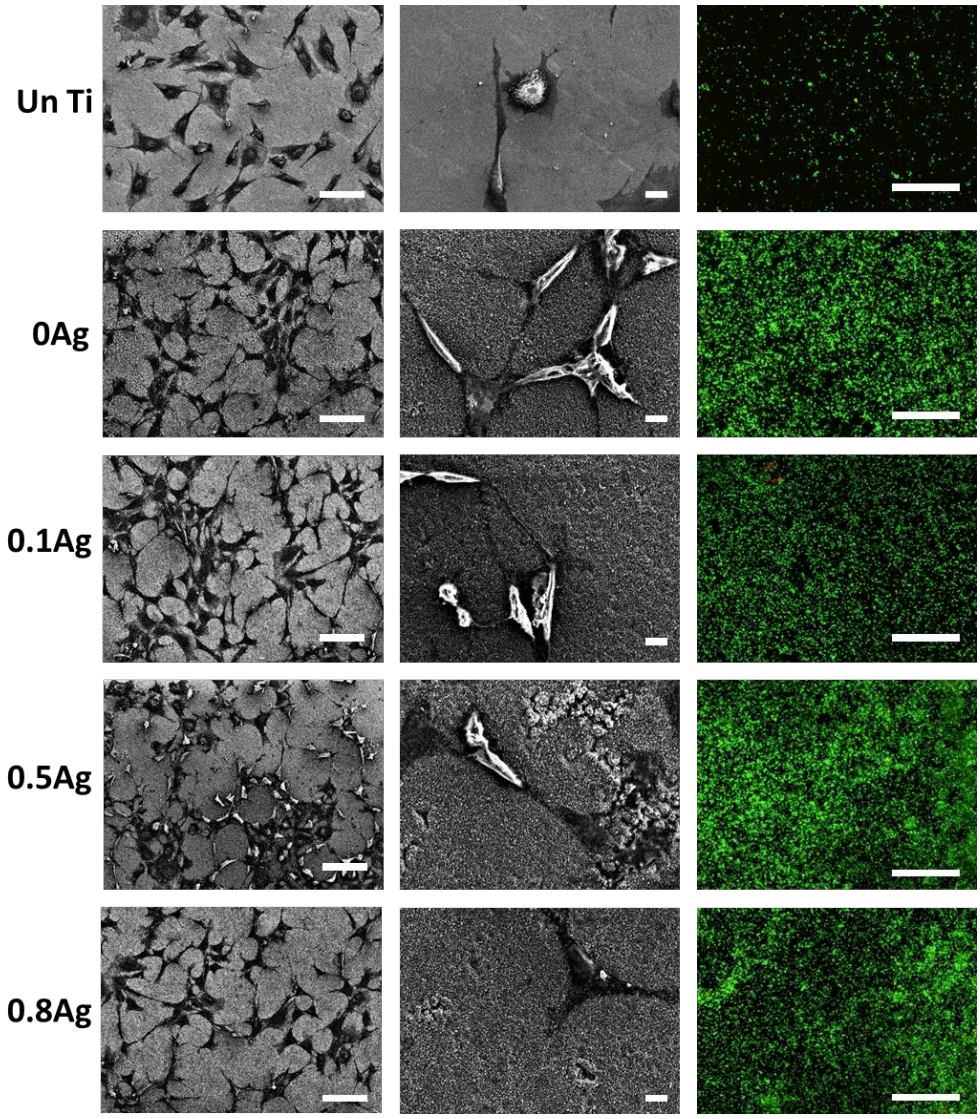

Figure 13. Fluorescence and SEM images of MC3T3 cells cultured on uncoated and coated Ti samples 1 day after cell seeding (scale bar: 100 µm (1st column), 10 µm (2nd column) and 500 µm (3rd column)).

Figure 14 shows the SEM and live/dead staining images obtained on untreated and PEO-treated Ti substrates seven days after cell seeding. The SEM images exhibited similar results as were observed one day after cell seeding: a significantly higher number of MC3T3 cells with a spread out morphology was observed on all PEO-treated samples in contrast to the untreated Ti sample which mainly showed the adherence of more round cells. However, the fluorescence images of

PEO-treated samples revealed that the viability of the osteoblast cells reduced when using the highest silver concentration in the coatings (sample 0.8Ag). Although there were no discernible dead cells found on the 0Ag, 0.1Ag and 0.5Ag coatings, a marked number of dead cells was present on the 0.8Ag coating suggesting possible cytotoxic effects of this particular coating.

The cellular response of the investigated samples are quantified using an MTT and the results are presented in **Figure 15.** This figure shows the viability of MC3T3 cells relative to TCPS one day and seven days after cell seeding for all investigated samples. It can be clearly seen that cell viability was higher on all PEO-treated samples than on untreated Ti. One day after cell seeding, there was no significant difference in cell viability between the 0Ag and 0.1Ag samples, both exhibiting approximately 80% cell viability. However, in the case of the 0.5Ag and 0.8Ag samples, the cell viability was slightly higher (around 93%). The obtained MTT results were thus in good agreement with the previously shown fluorescence images. Seven days after cell seeding, the cell viability increased further on all investigated samples with the exception of the 0.8Ag sample, on which cell viability reduced.

The observed differences in cellular response between the PEO treated and untreated Ti can be correlated to the surface wettability, roughness and chemical composition of the samples. The untreated Ti sample was less wettable and very smooth and thus showed poor protein adsorption and consequently a reduced osseointegration[62] compared to the PEO-treated samples. In fact, a very recent study suggested that a moderately hydrophilic (WCA in the range 20-40^{o}) and a roughened Ti surface exhibited the highest level of cell attachment[63,64]. Similar findings were also reported in several *in vivo* studies where rough surfaces were found to produce better bone fixation than smooth machined surfaces[62,65]. Consequently, the rough and more hydrophilic nature of the deposited coatings can thus explain the observed enhanced cell adhesion and growth. Moreover, the incorporation of Ca and P ions into the coatings also further enhanced the bioactivity of the coating. In fact, studies have reported that stoichiometric HA has a Ca/P ratio of 1.6 and that a

lower bioactivity was observed on HA coatings possessing Ca/P ratios below 1.5. From the XPS elemental composition (**Table 1**), it can be seen that the Ca/P ratio of the 0Ag, 0.1Ag, 0.5Ag and 0.8Ag coatings were 1.55, 1.45, 1.64 and 1.62, respectively, values which are close to the target ratio (Ca/P =1.6). Consequently, an increased bioactivity was seen on all PEO-treated samples irrespective of the silver content in the coating. However, among the PEO-treated coatings (0Ag, 0.1Ag, 0.5Ag and 0.8Ag), the observed difference in cell viability and proliferation was mainly related to the amount of Ag present on the coating surface and the increased crystalline phases since all coatings exhibited a similar wettability and surface roughness (see **Figure 7**). For example, the significant difference in cell viability 1 day after cell seeding between the 0Ag/0.1Ag samples and the 0.5Ag/0.8Ag samples and 7 days after cell seeding between the 0Ag and the 0.5Ag samples could be mainly attributed due to increased crystalline phases (rutile, hydroxyapatite, $CaTiO_3$) observed in the coatings with high Ag content (0.5Ag and/or 0.8Ag). Similar findings were reported by other researchers where an enhanced osseointegration was observed on a crystallized hydroxyapatite phase in comparison to an amorphous phase or a rutile TiO_2 coated material[66–68]. At this point, it is also important to note that the cumulative Ag^+ released from all the Ag-doped coatings under study during the first day was less than 400 ppb which is very significantly below the toxicity level for cells. However, 7 days after cell seeding, the 0.5Ag samples showed superior cell viability performance (Ag^+ release approximately 800 ppb), while the 0.8Ag samples showed lower cell viability. This may be due to the high Ag^+ release from this particular coating (> 1000 ppb) which potentially reduced the cell viability. However, based on our results, it can be seen that even on the 0.8Ag samples the cell viability was still above 70%, thereby meeting the ISO standards for an implant material to be biocompatible[69]. Hence, it can be stated that the PEO coatings developed in this study can provide an implant surface with a bi-functional character (antibacterial activity and tissue integration). On the other hand, there is an important trade-off between achieving the best antibacterial performance and the best cell viability

results. Indeed, the coatings with low amount of silver (0.1Ag) showed the best osteoblast cell response while exhibiting a lower 2 to 4 log reduction of bacteria (**Figure 10**). On the other hand, the osteoblast cell response was found to be lower when increasing the amount of silver (0.5Ag and 0.8Ag), but simultaneously the antibacterial performance also increased. Thus, finding an optimal balance between antibacterial efficacy and biocompatibility of the coatings is a crucial aspect when developing antibacterial PEO coatings. Only by maintaining the Ag^+ release sufficiently high to attain antibacterial efficacy, but still favorable for tissue integration over a long period of time, these coatings can be used for long term implantation. In a future study, more attention will therefore be paid to the Ag^+ release kinetics and osteoblast cell response over longer periods of time.

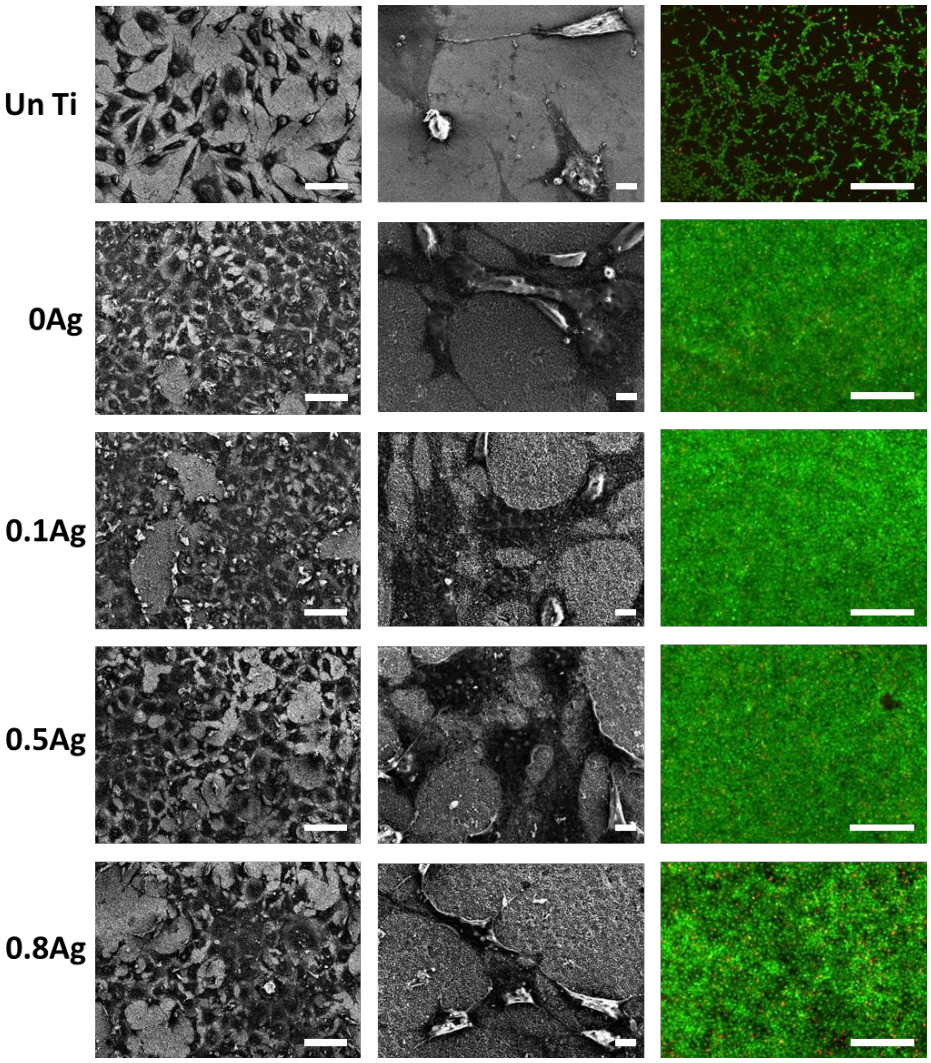

Figure 14. Fluorescent and SEM images of MC3T3 cells cultured on uncoated and coated Ti samples 7 days after cell seeding (scale bar: 100 μm (1st column), 10 μm (2nd column) and 500 μm (3rd column)).

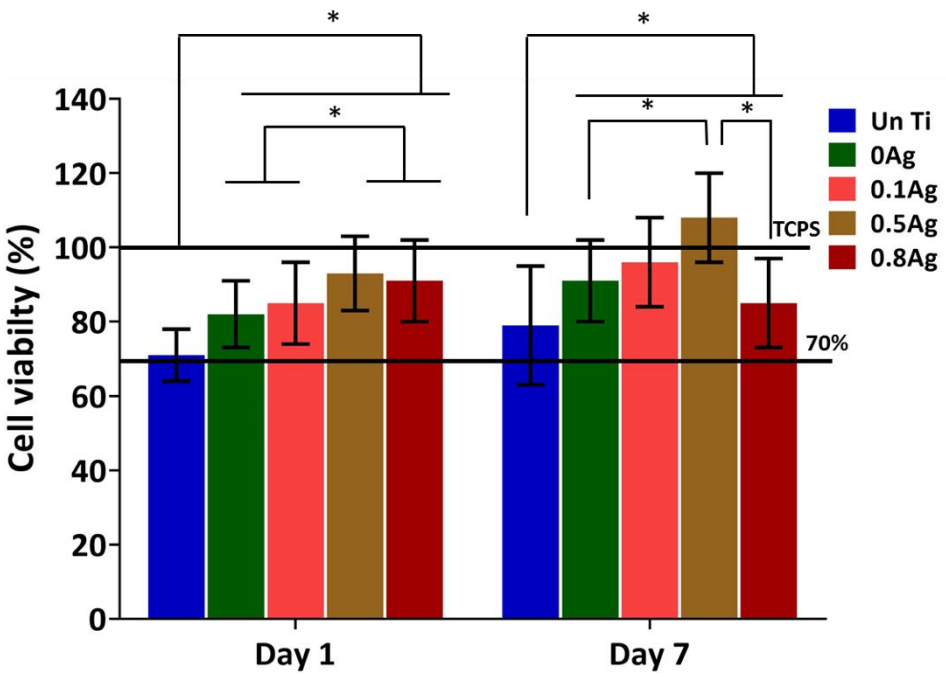

Figure 15. Cell viability results 1 day and 7 days after cell seeding on different titanium samples. Asterisk (*) denotes a significant difference at $P < 0.05$.

4. CONCLUSION

In the present study, the successful synthesis of bi-functional Ti surfaces by PEO has been demonstrated using an electrolyte enriched with calcium, phosphorus and silver acetate. For the first time, it was shown that crystalline phases such as rutile TiO_2 and Ca- and P-containing phases (hydroxyapatite, $CaTiO_3$) on the coating can be increased with increasing the silver acetate concentration in the electrolyte. This increased crystallinity was found to be a crucial factor in promoting successful protein adsorption and tissue integration. Increasing the silver acetate concentration in the electrolyte increased the silver content in the coatings from 0.8 at% to 2.2 at%. On the other hand, the porous microstructure of the coatings, their moderate surface roughness (0.8-1 μm) and high wettability (approximately 20°) were not altered by the incorporation of Ag. In addition, all PEO-treated coatings exhibited superior mechanical properties

i.e. improved microhardness and reduced frictional coefficient. The Ag^+ release characteristics of the Ag incorporated coatings in an aqueous environment were also examined and showed that the amount of Ag^+ released was dependent on the initial silver loading and the total incubation time. Due to this Ag^+ release, the Ag-doped coatings demonstrated excellent antibacterial efficiency against *E. coli*, MRSA and MSSA in comparison to the 0Ag coatings. Moreover, the antibacterial efficiency of the coating was observed to increase with an increase in silver acetate content in the electrolyte. Besides the very good antibacterial performance of the Ag-doped coatings, all prepared coatings were also able to facilitate tissue integration in comparison to the untreated Ti surface. Due to their superior mechanical properties, antibacterial efficacy and excellent biocompatibility, the produced coatings may be of significant interest for orthopedic implants. Therefore, future studies should assess interactions of different cells as well as bone formation on PEO-treated Ti surfaces and should focus on a tribocorrosion study to understand the degradation mechanisms of these coatings during implant applications. In addition, clinical trials will be needed to assess the longevity of the PEO-treated implant surfaces.

ASSOCIATED CONTENT

Supporting Information

The supporting information is available free of charge.

Methodology used for the *in vitro* antibacterial and cell culture experiments.

Figures showing the influence of silver acetate concentration on the current density of the PEO process and fluorescent images of studied coatings after incubation in FITC-labelled albumin (PDF).

AUTHOR INFORMATION

Corresponding Author

*E-mail: Monica.thukkaram@ugent.be; phone: 09-264-3829.

Author Contribution

M.T., design of research methodology, realization of experiments, data acquisition, processing, analyzing and writing of the original draft. R.C., data acquisition and processing. M.A., performing in vitro cell tests. P.T., performing XPS measurements. P.R., performing in vitro antibacterial tests. N.R., performing scratch test. A.N., R.M., A.T, L.W., K.V validation of all experiments, manuscript reviewing and correcting. J.S., validation of scratch test analysis. T.C., validation of antibacterial tests, manuscript reviewing and correcting. P.V., validation of XRD results, manuscript reviewing and correcting. G.L., validation of ICP-MS results, manuscript reviewing and correcting. P.B., validation of scratch test analysis, manuscript reviewing and correcting. N.G., funding acquisition, design of research methodology, validation of all experiments, manuscript reviewing and correcting.

ACKNOWLEDGMENTS

M.T. thanks the Research Foundation Flanders (FWO) for financing her PhD fellowship strategic basic research (1S13017N).

REFERENCES

(1) Prakasam, M.; Locs, J.; Salma-Ancane, K.; Loca, D.; Largeteau, A.; Berzina-Cimdina, L. Biodegradable Materials and Metallic Implants—A Review. *J. Funct. Biomater.* **2017**, *8* (4), 44. https://doi.org/10.3390/jfb8040044.

(2) Plecko, M.; Sievert, C.; Andermatt, D.; Frigg, R.; Kronen, P.; Klein, K.; Stübinger, S.; Nuss, K.; Bürki, A.; Ferguson, S.; Stoeckle, U.; Von Rechenberg, B. Osseointegration and Biocompatibility of Different Metal Implants--a Comparative Experimental Investigation in Sheep. *BMC Musculoskelet. Disord.* **2012**, *13*, 32. https://doi.org/10.1186/1471-2474-13-32.

(3) Albrich, W. C.; Angstwurm, M.; Bader, L.; Gärtner, R. Drug Resistance in Intensive Care Units. *Infection* **1999**, *27* (SUPPL. 2), 19–23. https://doi.org/10.1007/BF02561665.

(4) Haque, M.; Sartelli, M.; McKimm, J.; Abu Bakar, M. Health Care-Associated Infections - an Overview. *Infect. Drug Resist.* **2018**, *11*, 2321–2333. https://doi.org/10.2147/IDR.S177247.

(5) Thukkaram, M.; Cools, P.; Nikiforov, A.; Rigole, P.; Coenye, T.; Van Der Voort, P.; Du Laing, G.; Vercruysse, C.; Declercq, H.; Morent, R.; De Wilde, L.; De Baets, P.; Verbeken, K.; De Geyter, N. Antibacterial Activity of a Porous Silver Doped TiO2 Coating on Titanium Substrates Synthesized by Plasma Electrolytic Oxidation. *Appl. Surf. Sci.* **2020**, *500*. https://doi.org/10.1016/j.apsusc.2019.144235.

(6) He, X.; Zhang, X.; Wang, X.; Qin, L. Review of Antibacterial Activity of Titanium-Based Implants' Surfaces Fabricated by Micro-Arc Oxidation. *Coatings* **2017**, *7* (4), 45. https://doi.org/10.3390/coatings7030045.

(7) Zhang, T.; Wang, L.; Chen, Q.; Chen, C. Cytotoxic Potential of Silver Nanoparticles. *Yonsei Med. J.* **2014**, *55* (2), 283–291. https://doi.org/10.3349/ymj.2014.55.2.283.

(8) Qing, Y.; Cheng, L.; Li, R.; Liu, G.; Zhang, Y.; Tang, X.; Wang, J.; Liu, H.; Qin, Y. Potential Antibacterial Mechanism of Silver Nanoparticles and the Optimization of Orthopedic Implants by Advanced Modification Technologies. *Int. J. Nanomedicine* **2018**, *13*, 3311–3327. https://doi.org/10.2147/IJN.S165125.

(9) Prabhu, S.; Poulose, E. K. Silver Nanoparticles: Mechanism of Antimicrobial Action, Synthesis, Medical Applications, and Toxicity Effects. *Int. Nano Lett.* **2012**, *2* (1), 1–10. https://doi.org/10.1186/2228-5326-2-32.

(10) Coester, L. M.; Nepola, J. V; Allen, J.; Marsh, J. L. The Effects of Silver Coated External

Fixation Pins. *Iowa Orthop. J.* **2006**, *26*, 48–53.

(11) Panáček, A.; Kvítek, L.; Smékalová, M.; Večeřová, R.; Kolář, M.; Röderová, M.; Dyčka, F.; Šebela, M.; Prucek, R.; Tomanec, O.; Zbořil, R. Bacterial Resistance to Silver Nanoparticles and How to Overcome It. *Nat. Nanotechnol.* **2018**, *13* (1), 65–71. https://doi.org/10.1038/s41565-017-0013-y.

(12) Ahamed, M.; Alsalhi, M. S.; Siddiqui, M. K. J. Invited Critical Review Silver Nanoparticle Applications and Human Health. **2010**. https://doi.org/10.1016/j.cca.2010.08.016.

(13) Johnston, H. J.; Hutchison, G.; Christensen, F. M.; Peters, S.; Hankin, S.; Stone, V. A Review of the in Vivo and in Vitro Toxicity of Silver and Gold Particulates: Particle Attributes and Biological Mechanisms Responsible for the Observed Toxicity. *Critical Reviews in Toxicology*. April 2010, pp 328–346. https://doi.org/10.3109/10408440903453074.

(14) Kulkarni Aranya, A.; Pushalkar, S.; Zhao, M.; LeGeros, R. Z.; Zhang, Y.; Saxena, D. Antibacterial and Bioactive Coatings on Titanium Implant Surfaces. *J. Biomed. Mater. Res. - Part A* **2017**, *105* (8), 2218–2227. https://doi.org/10.1002/jbm.a.36081.

(15) Adeleke, S. A.; Sopyan, I.; Bushroa, A. R. Hydroxyapaptite Layer Formation on Titanium Alloys Surface Using Micro-Arc Oxidation. **2015**, *10* (21), 10101–10108.

(16) Kuroda, K.; Okido, M. Hydroxyapatite Coating of Titanium Implants Using Hydroprocessing and Evaluation of Their Osteoconductivity. *Bioinorg. Chem. Appl.* **2012**, *2012*, 730693. https://doi.org/10.1155/2012/730693.

(17) Thukkaram, M.; Vaidulych, M.; Kylián, O.; Hanuš, J.; Rigole, P.; Aliakbarshirazi, S.; Asadian, M.; Nikiforov, A.; Van Tongel, A.; Biederman, H.; Coenye, T.; Du Laing, G.; Morent, R.; De Wilde, L.; Verbeken, K.; De Geyter, N. Investigation of Ag/a-C:H

Nanocomposite Coatings on Titanium for Orthopedic Applications. *ACS Appl. Mater. Interfaces* **2020**, acsami.9b23237. https://doi.org/10.1021/acsami.9b23237.

(18) Zhao, L.; Chu, P. K.; Zhang, Y.; Wu, Z. Antibacterial Coatings on Titanium Implants. *J. Biomed. Mater. Res. - Part B Appl. Biomater.* **2009**, *91* (1), 470–480. https://doi.org/10.1002/jbm.b.31463.

(19) Yerokhin, A. L.; Nie, X.; Leyland, A.; Matthews, A.; Dowey, S. J. Plasma Electrolysis for Surface Engineering. *Surf. Coatings Technol.* **1999**, *122* (2–3), 73–93. https://doi.org/10.1016/S0257-8972(99)00441-7.

(20) Yerokhin, A. L.; Nie, X.; Leyland, A.; Matthews, A. Characterisation of Oxide Films Produced by Plasma Electrolytic Oxidation of a Ti–6Al–4V Alloy. *Surf. Coatings Technol.* **2000**, *130*, 195–206. https://doi.org/10.1016/S0257-8972(00)00719-2.

(21) Li, L. H.; Kong, Y. M.; Kim, H. W.; Kim, Y. W.; Kim, H. E.; Heo, S. J.; Koak, J. Y. Improved Biological Performance of Ti Implants Due to Surface Modification by Micro-Arc Oxidation. *Biomaterials* **2004**, *25* (14), 2867–2875. https://doi.org/10.1016/j.biomaterials.2003.09.048.

(22) Burghardt, I.; Lüthen, F.; Prinz, C.; Kreikemeyer, B.; Zietz, C.; Neumann, H. G.; Rychly, J. A Dual Function of Copper in Designing Regenerative Implants. *Biomaterials* **2015**, *44*, 36–44. https://doi.org/10.1016/j.biomaterials.2014.12.022.

(23) Chang, C.; Huang, X.; Liu, Y.; Bai, L.; Yang, X.; Hang, R.; Tang, B.; Chu, P. K. High-Current Anodization: A Novel Strategy to Functionalize Titanium-Based Biomaterials. *Electrochim. Acta* **2015**, *173*, 345–353. https://doi.org/10.1016/j.electacta.2015.05.075.

(24) Muhaffel, F.; Cempura, G.; Menekse, M.; Czyrska-Filemonowicz, A.; Karaguler, N.; Cimenoglu, H. Characteristics of Multi-Layer Coatings Synthesized on Ti6Al4V Alloy by

Micro-Arc Oxidation in Silver Nitrate Added Electrolytes. *Surf. Coatings Technol.* **2016**, *307*, 308–315. https://doi.org/10.1016/j.surfcoat.2016.09.002.

(25) Durdu, S.; Usta, M.; Berkem, A. S. Bioactive Coatings on Ti6Al4V Alloy Formed by Plasma Electrolytic Oxidation. *Surf. Coatings Technol.* **2016**, *301*, 85–93. https://doi.org/10.1016/j.surfcoat.2015.07.053.

(26) Xie, C.; Lu, H.; Li, W.; Chen, F. M.; Zhao, Y. M. The Use of Calcium Phosphate-Based Biomaterials in Implant Dentistry. *J. Mater. Sci. Mater. Med.* **2012**, *23* (3), 853–862. https://doi.org/10.1007/s10856-011-4535-9.

(27) Necula, B. S.; Apachitei, I.; Tichelaar, F. D.; Fratila-Apachitei, L. E.; Duszczyk, J. An Electron Microscopical Study on the Growth of TiO2-Ag Antibacterial Coatings on Ti6Al7Nb Biomedical Alloy. *Acta Biomater.* **2011**, *7* (6), 2751–2757. https://doi.org/10.1016/j.actbio.2011.02.037.

(28) Hu, H.; Zhang, W.; Qiao, Y.; Jiang, X.; Liu, X.; Ding, C. Antibacterial Activity and Increased Bone Marrow Stem Cell Functions of Zn-Incorporated TiO2 Coatings on Titanium. *Acta Biomater.* **2012**, *8* (2), 904–915. https://doi.org/10.1016/j.actbio.2011.09.031.

(29) Shalvoy, R. B.; Fisher, G. B.; Stiles, P. J. Bond Ionicity and Structural Stability of Some Average-Valence-Five Materials Studied by x-Ray Photoemission. *Phys. Rev. B* **1977**, *15* (4), 1680–1697. https://doi.org/10.1103/PhysRevB.15.1680.

(30) Sham, T. K.; Lazarus, M. S. X-Ray Photoelectron Spectroscopy (XPS) Studies of Clean and Hydrated TiO2 (Rutile) Surfaces. *Chem. Phys. Lett.* **1979**, *68* (2–3), 426–432. https://doi.org/10.1016/0009-2614(79)87231-0.

(31) Kasuga, T.; Kondo, H.; Nogami, M. Apatite Formation on TiO2 in Simulated Body Fluid.

J. Cryst. Growth **2002**, *235* (1–4), 235–240. https://doi.org/10.1016/S0022-0248(01)01782-1.

(32) Moulder, J. F.; Stickle, W. F.; Sobol, P. E. ’; Bomben, K. D.; Chastain, J. *Handbook of X-Ray Photoelectron Spectroscopy AReference Book of Standard Spectra for Identification and Interpretation of XPS Data*.

(33) Han, Y.; Chen, D.; Sun, J.; Zhang, Y.; Xu, K. UV-Enhanced Bioactivity and Cell Response of Micro-Arc Oxidized Titania Coatings. *Acta Biomater.* **2008**, *4* (5), 1518–1529. https://doi.org/10.1016/J.ACTBIO.2008.03.005.

(34) Song, W.-H.; Ryu, H. S.; Hong, S.-H. Antibacterial Properties of Ag (or Pt)-Containing Calcium Phosphate Coatings Formed by Micro-Arc Oxidation. *J. Biomed. Mater. Res. Part A* **2009**, *88A* (1), 246–254. https://doi.org/10.1002/jbm.a.31877.

(35) López-Huerta, F.; Cervantes, B.; González, O.; Hernández-Torres, J.; García-González, L.; Vega, R.; Herrera-May, A. L.; Soto, E. Biocompatibility and Surface Properties of TiO2 Thin Films Deposited by DC Magnetron Sputtering. *Materials (Basel).* **2014**, *7* (6), 4105–4117. https://doi.org/10.3390/ma7064105.

(36) Durdu, S.; Deniz, Ö. F.; Kutbay, I.; Usta, M. Characterization and Formation of Hydroxyapatite on Ti6Al4V Coated by Plasma Electrolytic Oxidation. *J. Alloys Compd.* **2013**, *551*, 422–429. https://doi.org/10.1016/j.jallcom.2012.11.024.

(37) Stanishevsky, A. V.; Holliday, S. Mechanical Properties of Sol-Gel Calcium Titanate Bioceramic Coatings on Titanium. *Surf. Coatings Technol.* **2007**, *202* (4–7), 1236–1241. https://doi.org/10.1016/j.surfcoat.2007.07.091.

(38) Zhang, L.; Guo, J.; Huang, X.; Zhang, Y.; Han, Y. The Dual Function of Cu-Doped TiO_2 Coatings on Titanium for Application in Percutaneous Implants. *J. Mater. Chem. B* **2016**, *4*

(21), 3788–3800. https://doi.org/10.1039/C6TB00563B.

(39) Siva Rama Krishna, D.; Brama, Y. L.; Sun, Y. Thick Rutile Layer on Titanium for Tribological Applications. *Tribol. Int.* **2007**, *40* (2 SPEC. ISS.), 329–334. https://doi.org/10.1016/j.triboint.2005.08.004.

(40) Oliver, W. C.; Hutchings, R.; Pethica, J. B. WEAR BEHAVIOR OF NITROGEN-IMPLANTED METALS. *Metall. Trans. A, Phys. Metall. Mater. Sci.* **1984**, *15 A* (12), 2221–2229. https://doi.org/10.1007/BF02647105.

(41) Nasiri Vatan, H.; Ebrahimi-Kahrizsangi, R.; Kasiri-Asgarani, M. Wear and Corrosion Performance of Peo-Synthesized Sic Nanocomposite Coatings: Effect of Processing Time and Current Density. *Int. J. Electrochem. Sci.* **2016**, *11* (7), 5631–5654. https://doi.org/10.20964/2016.07.17.

(42) Li, J.; Zhang, X.; Wang, J.; Li, H.; Huang, J.; Xiong, D. Frictional Properties of Silver Over-Coated on Surface Textured Tantalum Interlayer at Elevated Temperatures. *Surf. Coatings Technol.* **2019**, *365*, 189–199. https://doi.org/10.1016/j.surfcoat.2018.10.067.

(43) Kumar, C. A. V.; Rajadurai, J. S. Influence of Rutile (TiO2) Content on Wear and Microhardness Characteristics of Aluminium-Based Hybrid Composites Synthesized by Powder Metallurgy. *Trans. Nonferrous Met. Soc. China (English Ed.* **2016**, *26* (1), 63–73. https://doi.org/10.1016/S1003-6326(16)64089-X.

(44) Arash, V.; Anoush, K.; Rabiee, S. M.; Rahmatei, M.; Tavanafar, S. The Effects of Silver Coating on Friction Coefficient and Shear Bond Strength of Steel Orthodontic Brackets. *Scanning* **2015**, *37* (4), 294–299. https://doi.org/10.1002/sca.21212.

(45) Zhu, J.; Xu, M.; Yang, W.; Li, D.; Zhou, L.; Fu, L. Friction and Wear Behavior of an Ag–Mo Co-Implanted GH4169 Alloy via Ion-Beam-Assisted Bombardment. *Coatings* **2017**, *7*

(11), 191. https://doi.org/10.3390/coatings7110191.

(46) Abu-Amer, Y.; Darwech, I.; Clohisy, J. C. Aseptic Loosening of Total Joint Replacements: Mechanisms Underlying Osteolysis and Potential Therapies. *Arthritis Research and Therapy*. BioMed Central June 29, 2007, p S6. https://doi.org/10.1186/ar2170.

(47) Damm, N. B.; Morlock, M. M.; Bishop, N. E. Friction Coefficient and Effective Interference at the Implant-Bone Interface. *J. Biomech.* **2015**, *48* (12), 3517–3521. https://doi.org/10.1016/j.jbiomech.2015.07.012.

(48) Abdullaeva, Z. *Nano-and Biomaterials: Compounds, Properties, Characterization, and Applications*; 2017.

(49) Shi, C.; Gao, J.; Wang, M.; Fu, J.; Wang, D.; Zhu, Y. Ultra-Trace Silver-Doped Hydroxyapatite with Non-Cytotoxicity and Effective Antibacterial Activity. *Mater. Sci. Eng. C* **2015**, *55*, 497–505. https://doi.org/10.1016/J.MSEC.2015.05.078.

(50) Greulich, C.; Kittler, S.; Epple, M.; Muhr, G.; Köller, M. Studies on the Biocompatibility and the Interaction of Silver Nanoparticles with Human Mesenchymal Stem Cells (HMSCs). *Langenbeck's Arch. Surg.* **2009**, *394* (3), 495–502. https://doi.org/10.1007/s00423-009-0472-1.

(51) Rai, M.; Yadav, A.; Gade, A. Silver Nanoparticles as a New Generation of Antimicrobials. *Biotechnol. Adv.* **2009**, *27* (1), 76–83. https://doi.org/10.1016/j.biotechadv.2008.09.002.

(52) Jung, W. K.; Koo, H. C.; Kim, K. W.; Shin, S.; Kim, S. H.; Park, Y. H. Antibacterial Activity and Mechanism of Action of the Silver Ion in Staphylococcus Aureus and Escherichia Coli. *Appl. Environ. Microbiol.* **2008**, *74* (7), 2171–2178. https://doi.org/10.1128/AEM.02001-07.

(53) Sondi, I.; Salopek-Sondi, B. Silver Nanoparticles as Antimicrobial Agent: A Case Study on

E. Coli as a Model for Gram-Negative Bacteria. *J. Colloid Interface Sci.* **2004**, *275* (1), 177–182. https://doi.org/10.1016/j.jcis.2004.02.012.

(54) Liu, J.; Hurt, H. R. Ion Release Kinetics and Particle Persistence in Aqueous Nano-Silver Colloids. *Environ. Sci. Technol.* **2010**, *44*, 2169–2175. https://doi.org/10.1021/es9035557.

(55) Lorenzetti, M.; Bernardini, G.; Luxbacher, T.; Santucci, A.; Kobe, S.; Novak, S. Surface Properties of Nanocrystalline TiO2 Coatings in Relation to the in Vitro Plasma Protein Adsorption. *Biomed. Mater.* **2015**, *10* (4), 045012. https://doi.org/10.1088/1748-6041/10/4/045012.

(56) Takami, Y.; Yamane, S.; Makinouchi, K.; Otsuka, G.; Glueck, J.; Benkowski, R.; Nosé, Y. Protein Adsorption onto Ceramic Surfaces. *J. Biomed. Mater. Res.* **1998**, *40* (1), 24–30. https://doi.org/10.1002/(SICI)1097-4636(199804)40:1<24::AID-JBM3>3.0.CO;2-T.

(57) Chen, K.; Ustriyana, P.; Moore, F.; Sahai, N. Biological Response of and Blood Plasma Protein Adsorption on Silver-Doped Hydroxyapatite. **2019**. https://doi.org/10.1021/acsbiomaterials.8b00996.

(58) Sun, Z. L.; Bai, L.; Guan, G. P.; Zhuan, K. H.; Dai, H. Q. Protein Adsorption and Biocompatibility of Porous Silk Fiboin Films. In *Proceedings of the 2009 2nd International Conference on Biomedical Engineering and Informatics, BMEI 2009*; 2009. https://doi.org/10.1109/BMEI.2009.5305691.

(59) Wang, X.; Herting, G.; Odnevall Wallinder, I.; Blomberg, E. Adsorption of Bovine Serum Albumin on Silver Surfaces Enhances the Release of Silver at PH Neutral Conditions. *Phys. Chem. Chem. Phys.* **2015**, *17* (28), 18524–18534. https://doi.org/10.1039/c5cp02306h.

(60) Zeng, H.; Chittur, K. K.; Lacefield, W. R. *Analysis of Bovine Serum Albumin Adsorption on Calcium Phosphate and Titanium Surfaces*; 1999; Vol. 20.

(61) Shen, X. C.; Liang, H.; Guo, J. H.; Song, C.; He, X. W.; Yuan, Y. Z. Studies on the Interaction between Ag+ and Human Serum Albumin. *J. Inorg. Biochem.* **2003**, *95* (2–3), 124–130. https://doi.org/10.1016/S0162-0134(03)00094-1.

(62) Hara, T.; Matsuoka, K.; Matsuzaka, K.; Yoshinari, M.; Inoue, T. Effect of Surface Roughness of Titanium Dental Implant Placed under Periosteum on Gene Expression of Bone Morphogenic Markers in Rat. *Bull. Tokyo Dent. Coll.* **2012**, *53* (2), 45–50. https://doi.org/10.2209/tdcpublication.53.45.

(63) Hara, T.; Matsuoka, K.; Matsuzaka, K.; Yoshinari, M.; Inoue, T. Effect of Surface Roughness of Titanium Dental Implant Placed under Periosteum on Gene Expression of Bone Morphogenic Markers in Rat. *Bull. Tokyo Dent. Coll.* **2012**, *53* (2), 45–50. https://doi.org/10.2209/tdcpublication.53.45.

(64) Novaes, A. B.; de Souza, S. L. S.; de Barros, R. R. M.; Pereira, K. K. Y.; Iezzi, G.; Piattelli, A. Influence of Implant Surfaces on Osseointegration. *Brazilian Dental Journal*. 2010, pp 471–481. https://doi.org/10.1590/s0103-64402010000600001.

(65) Braun, G.; Kohavi, D.; Amir, D.; Luna, M.; Caloss, R.; Sela, J.; Dean, D. D.; Boyan, B. D.; Schwartz, Z. Markers of Primary Mineralization Are Correlated with Bone-bonding Ability of Titanium or Stainless Steel in Vivo. *Clin. Oral Implants Res.* **1995**, *6* (1), 1–13. https://doi.org/10.1034/j.1600-0501.1995.060101.x.

(66) Zhang, X.; Wu, Y.; Lv, Y.; Yu, Y.; Dong, Z. Formation Mechanism, Corrosion Behaviour and Biological Property of Hydroxyapatite/TiO2 Coatings Fabricated by Plasma Electrolytic Oxidation. *Surf. Coatings Technol.* **2020**, *386*, 125483. https://doi.org/10.1016/j.surfcoat.2020.125483.

(67) Wang, G.; Li, J.; Lv, K.; Zhang, W.; Ding, X.; Yang, G.; Liu, X.; Jiang, X. Surface Thermal Oxidation on Titanium Implants to Enhance Osteogenic Activity and in Vivo

Osseointegration. *Sci. Rep.* **2016**, *6* (March), 1–13. https://doi.org/10.1038/srep31769.

(68) Tsou, H.-K.; Hsieh, P.-Y.; Chi, M.-H.; Chung, C.-J.; He, J.-L. Improved Osteoblast Compatibility of Medical-Grade Polyetheretherketone Using Arc Ionplated Rutile/Anatase Titanium Dioxide Films for Spinal Implants. *J Biomed Mater Res Part A* **2012**, *100*, 2787–2792. https://doi.org/10.1002/jbm.a.34215.

(69) ISO - ISO 10993-5:2009 - Biological evaluation of medical devices — Part 5: Tests for in vitro cytotoxicity https://www.iso.org/standard/36406.html (accessed Dec 17, 2019).

Table of contents (TOC) graph

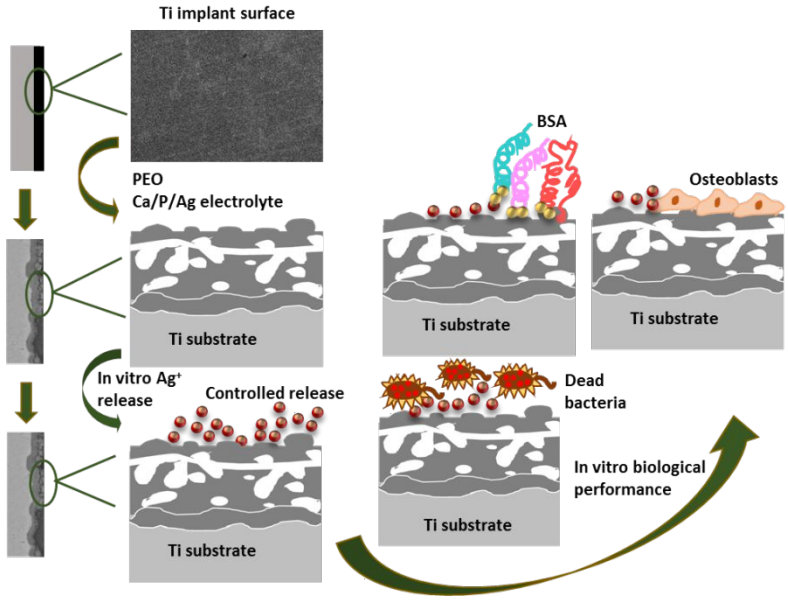

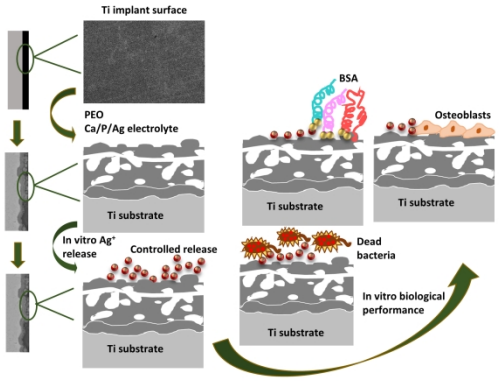

338x190mm (300 x 300 DPI)